

ABSTRACT

Title of Thesis: UNDERFILL SELECTION TO IMPROVE
SOLDER JOINT RELIABILITY FOR DOWN
HOLE DRILLING APPLICATIONS

Sriram Jayanthi, Master of Science, 2020

Thesis Directed By: Professor, Patrick McCluskey, Mechanical
Engineering

Underfill materials were originally developed to improve the solder joint reliability of the BGA packages under the thermal cycling when they are experiencing stresses due to the CTE mismatches between the board and the component. Although it is stated that the underfills will improve the shock reliability of the solder joints under the harsh environment for automobiles and military applications (-40 to 125°C). It has been found in the thermal cycling conditions the underfills will reduce the life of the solder balls.

All the studies that had been performed were mostly below 150°C. There are no certain guidelines for selecting the underfills with the properties of the materials. The main aim of this research is to create a guideline for selecting the underfills for high temperature applications (above 150°C) for different BGA packages. In the first section initial characterization and benchmarking of the underfills that are available in the industry was performed. In the second section, all the selected underfills were subjected to a harsh environment to find the failure modes and mechanisms. With the help of

experimentation and FEA that was done, guidelines were created for selecting the underfills for different BGA packages. This will be helpful to oil & gas and military applications.

UNDERFILL SELECTION TO IMPROVE SOLDER JOINT RELIABILITY FOR
DOWN HOLE DRILLING APPLICATIONS

by

SRIRAM JAYANTHI

Thesis submitted to the Faculty of the Graduate School of the
University of Maryland, College Park, in partial fulfillment
of the requirements for the degree of
Master of Science
2020

Advisory Committee:
Professor, Patrick McCluskey, Chair
Professor, Abhijit Das Gupta
Dr. Michael Azarian

© Copyright by
Sriram Jayanthi
2020

Dedication

To my parents, sister, and friends for their unwavering support
throughout my journey as a master's student.

Acknowledgements

I would like to thank my advisor Prof. Patrick McCluskey for his unwavering support throughout my graduate studies. I would also thank my committee members Abhijit Dasgupta and Michael H. Azarian for their guidance in my research.

I would also like to thank members of Prof. McCluskey group Subramani Manoharan, Erick Gutierrez, Yonatan Saadon, Zhaoxi Yao, He Yun, Gilad, and Cliff for sharing their expertise and helping me with my research.

Table of Contents

Dedication.....	ii
Acknowledgements.....	iii
Table of Contents.....	iv
List of Tables.....	v
List of Figures.....	vi
Introduction.....	1
Thermo mechanical failures in solder balls.....	1
Application of the Underfill to a BGA package.....	2
Problem Statement and scope of thesis.....	4
Literature Review.....	5
Effect of Underfill properties on the fatigue life of the solder balls.....	5
Experimental Setup.....	11
Background.....	11
Design of Experiment.....	16
Test Vehicle.....	19
Environmental Testing.....	21
Data Analysis.....	24
ANOVA Analysis.....	30
Finite Element Analysis.....	32
Failure Analysis.....	40
Non-Destructive Analysis.....	40
Destructive Analysis.....	43
Optical Microscopy.....	44
EDS Analysis for all the Packages.....	45
SEM Analysis.....	47
Failure Analysis Conclusions.....	59
Material Characterization.....	61
Aging Test.....	61
TMA Testing.....	62
DMA Testing.....	68
Hypothesis.....	73
Verification.....	74
Conclusions.....	74
Guidelines for selecting the underfills.....	74
Contributions.....	75
Bibliography.....	76

List of Tables

Table 1: Field conditions for different electronic industries.....	2
Table 2: Properties of the underfill materials selected for the study [17].....	6
Table 3: Crack length measurement of the solder joints after the thermal cycling [17]6	
Table 4: Underfills properties and thermal cycling results of CBGA's [19].....	8
Table 5: Predicted and measured values of characteristic life of five CBGA assemblies [19].....	8
Table 6: Underfill properties and configurations (fully filled and corner bonding) [21]	10
Table 7: Weibull parameter estimates for thermal cycling experiment [21]	10
Table 8: Resin in the underfills that were benchmarked.....	12
Table 9: Properties of the corner bonded underfill materials used for preliminary FEA analysis.....	13
Table 10: Properties of the fully filled underfill materials used for preliminary FEA analysis.....	15
Table 11: Number of boards of each underfill that was used for the experimentation	19
Table 12: Definition of the failure with the change in the voltage values	21
Table 13: First TTF of each component that was collected from the in-situ monitoring	26
Table 14: Data considered for the ANOVA Analysis	31
Table 15: Results of the Analysis for different Underfill Materials	31
Table 16: Results of the ANOVA Analysis	31
Table 17: Design of Experiment for the aging test	62
Table 18: Comparison between experimental and data sheet value of Henkel material	63
Table 19: TMA results of bulk Henkel samples aged at 200 °C.....	64
Table 20: TMA results of Henkel samples aged at room temperature	65
Table 21: Comparison between experimental and data sheet value of Sanyu material	66
Table 22: TMA results of bulk Sanyu samples aged at 200 °C.....	67
Table 23: Comparison between experimental and data sheet value of Henkel material	69
Table 24: DMA results of bulk Henkel samples aged at 200 °C.....	70
Table 25: Comparison between experimental and data sheet value of Sanyu material	71
Table 26: DMA results of bulk Sanyu samples aged at 200 °C	72

List of Figures

Figure 1: Different underfill configurations	3
Figure 2: Cracking at the interface after 500 thermal cycles (-40 to 125 °C) [17].....	6
Figure 3: Different package types used in the study [18]	7
Figure 4: Weibull analysis results of the study for different configurations [20].....	9
Figure 5: All the commercially available underfills in the industry	11
Figure 6: Results of the preliminary FEA analysis for the corner bonded materials..	14
Figure 7: Results of the preliminary FEA analysis for the fully filled underfill materials	15
Figure 8: Preliminary FEA analysis prediction of all the material that were selected for the experiment	16
Figure 9: Designs of different boards with packages that were considered for the experiment.....	17
Figure 10: Final design of the board with components that was used in the experimentation.....	18
Figure 11: Circuit diagram of the resistors that was present on the board that was used for 1 wire measurement	20
Figure 12: Thermal cycling profile used in the experiment.....	22
Figure 13: Arrangement of the boards in the environmental chamber with all the thermocouple.....	23
Figure 14: Identification of the failure from the in-situ monitoring data and comparison between the three thermocouples	24
Figure 15: Weibull analysis results of all the components that went through thermal cycling test	28
Figure 16: Graphical representation of the results with 95% C.I	32
Figure 17: Depiction of the quarter symmetrical model with cut sections and the copper pads	33
Figure 18: Boundary conditions that were applied to the quarter symmetrical model	33
Figure 19: Plastic work across the solder balls for the No UF condition	35
Figure 20: Failure in the BGA packages found through probing for the boards without UF	36
Figure 21: Half symmetrical model created for the UF case to include the warpage stresses	37
Figure 22: Plastic work across the solder balls in a UF board with the warpage stresses	38
Figure 23: Failures in the BGA packages found through probing for the boards with UF	39
Figure 24: Graphical representation of the connections between the solder balls and the daisy chains in the BGA packages	41
Figure 25: Failures found in the package with probing after the experiment	42
Figure 26: Steps for performing the failure analysis	44
Figure 27: EDS analysis on the board side of the package for the verification of the nickel barrier	45

Figure 28: EDS analysis on the component side of the package for the verification of the nickel barrier	46
Figure 29: Plastic work across the solder ball for the No UF component to find out the critical solder ball.....	48
Figure 30: Failures in the solder ball due to the warpage stresses acting on the packages.....	48
Figure 31: Failures in the CSP devices, the crack is initiated on the component side	49
Figure 32: Failures in the lord material packages, as they are concentrated on the corners of the package	50
Figure 33: Failures occurred in the solder balls due to the tensile stresses in the lord material packages.....	51
Figure 34: Early failure in the Henkel material due to weak substrate.....	52
Figure 35: Voids present under the package with the Henkel underfill	53
Figure 36: Cracks found in the die attach and the underfill in the failure analysis	55
Figure 37: Solder extrusions found on the component side due to the continuous expansion and contraction of the underfill.....	56
Figure 38: Solder ball failures found in the Henkel material packages due to the combination of shear and tensile stresses	57
Figure 39: Failure sites found in the packages with Sanyu material under the thermal cycling.....	58
Figure 40: TMA equipment used for measuring the properties.....	62
Figure 41: Time 0 TMA result of Henkel material.....	63
Figure 42: Graphical representation of the Henkel's TMA results.....	65
Figure 43: Time 0 TMA result of Sanyu material	66
Figure 44: Graphical representation of the Sanyu TMA results	68
Figure 45: DMA tensile testing.....	68
Figure 46: Time 0 DMA result of Henkel material	69
Figure 47: Graphical representation of the Henkel's DMA results	70
Figure 48: Time 0 DMA result of Sanyu material.....	71
Figure 49: Graphical representation of the Sanyu DMA results.....	72
Figure 50: Graphical representation of the TMA results showing the reduction in T_g over a period of aging in Sanyu material	73
Figure 51: TTF values of the BGA packages with the changed material properties..	74

Introduction

Thermo mechanical failures in solder balls

Solder balls are the most important second level interconnects in the BGA packages.

Their main application is to join the BGA package electrically and mechanically to the printed circuit board (PCB). Solder balls will experience stresses when the package is going through its intended life cycle conditions, resulting in the failures of the solder balls. The solder balls will experience stresses due to the local and global CTE mismatches between the component and the board. These stresses are dominant when the component is undergoing through a thermal cycle. The US air force performed a study to quantify the failures observed in the field to different stress conditions, they identified that 55% of the failures are due to the high temperature and thermal cycling, 20% are due to mechanical vibration and shock and 20% are due to humidity [1]. During a thermal cycle solder balls will experience shear stresses due to the CTE mismatch between the package and the board. The large CTE mismatches can cause fatigue failures in the solder balls. In the surface mount packages the corner solder balls will experience maximum amount of shear stresses due to the Distance from the neutral point (DNP). Due to the package warpage and the local CTE mismatches the solder balls farther from the neutral point will experience maximum stresses. This effect will be predominant in the larger package sizes [2,3].

In most of the life cycle conditions the components will only experience thermal cycling conditions from -40 to 125 °C. Table 1 will present the different thermal cycle field conditions for different electronic industries [4][5][6]. For most of the applications

the accelerated life testing will be performed from -40 to 125 °C [7]. Although life cycles profiles might vary for different applications the studies that was mostly performed previously were below 150 °C.

	Temp range	Cycles/year	Service time	Failure rate
Consumer	0 to 60 °C	365	1 year	1 %
Computer	15 to 60 °C	1460	5 years	0.1 %
Telecom	-40 to 85 °C	365	7 to 20 years	0.01 %
Aircraft	-55 to 95 °C	365	20 years	0.001 %
Automotive	-55 to 95 °C	100	10 years	0.1 %

Table 1: Field conditions for different electronic industries

As the solder balls undergoing through a thermal cycle with long dwell times, low cycle fatigue failures will be occurred. After continuous thermal cycle the crack will be nucleated due to the stresses acting on the solder balls resulting in the crack propagation along the grain boundaries resulting in open circuit [8].

Application of the Underfill to a BGA package

Underfill materials were originally developed to improve the solder joint reliability of the BGA packages under the thermal cycling. It was mainly recognized after the introduction of the C4 bumps introduced by the IBM [9]. There is lot of research performed on the reliability of the solder balls with the underfill under the package. It was mentioned in the literature that the underfills with low CTE, high T_g and high modulus would perform better in a thermal cycle condition but all the studies that was performed were below 150 °C [10]. In most applications underfills will be used to support the solder balls from the stresses by creating a uniform continuous layer below the substrate, which will distribute all the stresses that were acting on the solder balls.

This was proven wrong as in some cases it was found that the Underfill might increase or decrease reliability of the BGA package [11,12]. There are different configurations in which the underfills can be applied under the BGA packages (fully filled, edge bonding and corner stacking). Each configuration will have its own advantages and disadvantages. Figure 1 explains all the configurations of the underfills.

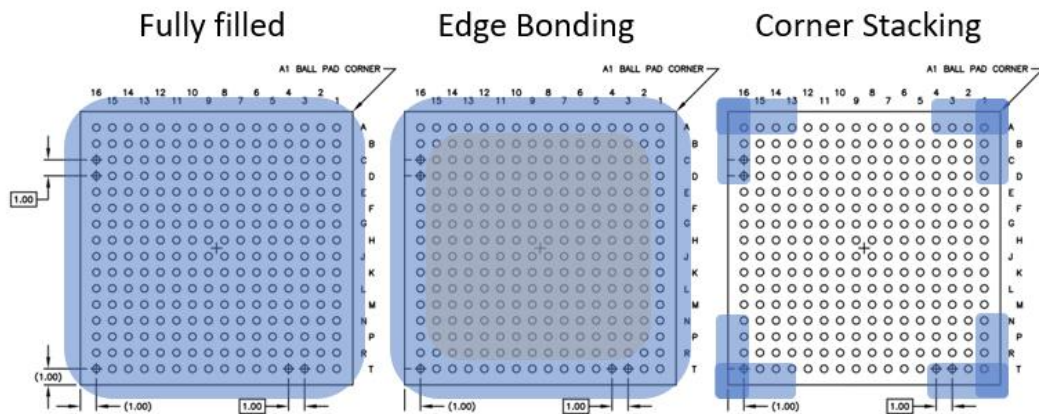


Figure 1: Different underfill configurations

Corner bonding material uses very low material, which will incur low production pad costs, but it will not provide full support from the moisture and contamination. Fully filled will give the complete protection to the solder balls but the cost will be high. Edge bonding will not give full protection to the solder balls, but it will use less material compared to the fully filled condition.

The selection of the underfills will play a vital role in the reliability of the solder balls. When the underfill cures there might be a chance of voiding and delamination, reducing the reliability of the package by increasing the stresses concentrations in these areas [13,14]. The properties of the material were extensively studied in the literature, it is found that the materials with low CTE would improve the thermo mechanical reliability of the BGA packages [15]. Although it is stated in the literature that the high T_g

materials will increase the reliability of the BGA, it will also increase the risk of low-k cracking [16]. It is also stated that the low T_g materials will decrease the reliability of the BGA packages [17,18]. This will create the uncertainty about the guidelines that was created for selecting the underfill. The important point that should be noted is that all the guidelines that were created is for the low thermal cycling conditions below 150 °C.

Problem Statement and scope of thesis

Although previous studies mentioned that the Underfills with low CTE, high T_g and high modulus would perform better in the thermal cycling conditions. There is ambiguity in the studies that were performed, which will make the decision of selection of underfill difficult in the industry. Most of the studies that was performed was for low temperature applications below 150 °C. There are no clear guidelines for selecting the underfills according to their properties that were mentioned in the data sheets. This research was done to address this gap in the literature by creating guidelines for selecting the underfills for high temperature applications. This research will be useful to oil and gas and military applications.

Literature Review

Solder balls under the BGAs will experience stresses due to the CTE mismatch between the component and the board under a thermal cycle. There is a lot of research focused on the stresses that were acting on the solder balls and fatigue life of the solder balls under the BGA packages. This chapter will focus on the effect of underfill on the fatigue life of the solder balls and explains the extent of the current research and the research gaps that are present. It will also cover the effect of underfill properties on the fatigue life of the BGA packages.

Effect of Underfill properties on the fatigue life of the solder balls

In the previous studies, reliability test for the BGA packages with different underfill properties were performed. Bo-In Noh et al. studied 9mm * 9mm packages with three underfills of varying CTE. All the packages were subjected to a thermal cycling test from -40 to 125 °C resulting in the interfacial failure at the solder ball – bond pad interface which is shown in figure 2. Crack length measurements indicated that a lower CTE underfills has a lower crack propagation rate compared to the one with higher CTE [19]. The properties of the materials that were taken for the experiment is presented in Table 2. The point that should be noted is that the underfills that were tested in this study has very low T_g and the CTE of the materials is very high.

Table 3 will show all the crack length measurements taken after the thermal cycling experiment

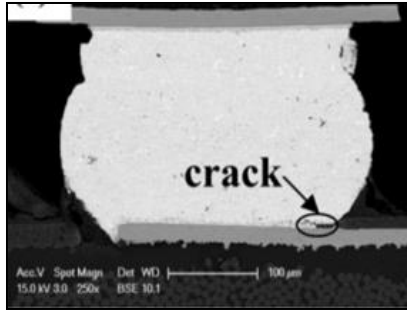


Figure 2: Cracking at the interface after 500 thermal cycles (-40 to 125 °C) [19]

Underfill	CTE (ppm/°C)	T _g (°C)
A	94	95
	96	
B	152	74
	189	
C	160	68
	195	

Table 2: Properties of the underfill materials selected for the study [19]

CRACK LENGTH OF SOLDER JOINTS ACCORDING TO THE THERMAL SHOCK CYCLE				
	0 cycle	200 cycle	500 cycle	1000 cycle
no-underfill	0	65	80	120
underfill A	0	21	42	56
underfill B	0	30	55	94
underfill C	0	46	60	103

(unit: μm)

Table 3: Crack length measurement of the solder joints after the thermal cycling [19]

Another study conducted by Nokibul Islam et al. tested bare die CSP devices and the flip chip packages under at thermal cycling experiment and found that the underfills will increase the fatigue life of the flip chip bumps more than the CSP devices. It tells us that the underfills will work better for the 2nd level solder interconnects than the CSP devices [20].

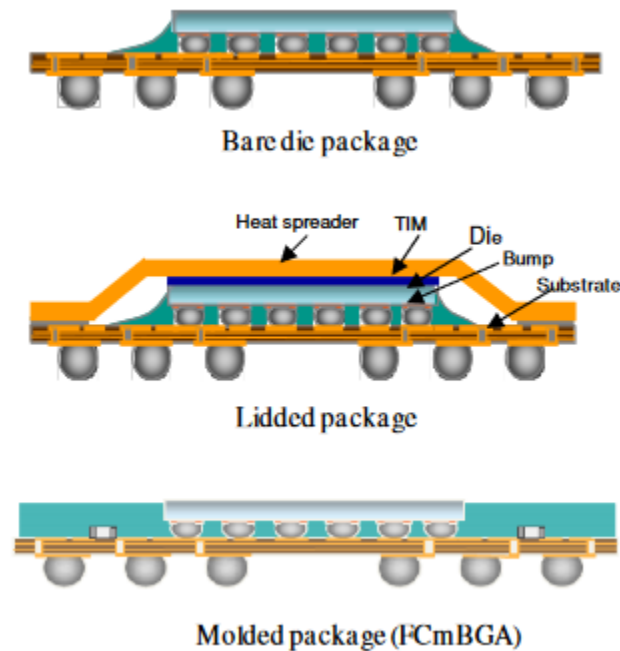


Figure 3: Different package types used in the study [18]

Burnette et al. conducted a study on the ceramic packages to check the effect of underfill properties on the reliability of the ceramic packages. Different underfills with varying CTE and the modulus was taken into consideration and the packages were subjected to a thermal cycling test from 0 to 100°C. A FEA analysis was also performed to verify the results that was presented in the study, which explains the important of the temperature dependent properties of the underfills. Table 4 will explain all the underfills that were taken and results of the test. After the experiment it was found that the underfill will increase the fatigue life of the ceramic packages drastically [21]. It is

stated in the study that the modulus of the underfill has no detrimental effect on the fatigue life of the solder balls and the CTE of the material plays a vital role in the increase of the fatigue life.

Epoxy	CTE	Modulus
A	75	2.6
B	44	5.6
C	40	8.5
D	26	5.5

Epoxy	50%	1%	0.1%
Control	2426	1980	1851
A	2070	931	713
B	5160	3013	2518
C	5097	3100	2626
D	No Fails		

Table 4: Underfills properties and thermal cycling results of CBGA's [21]

The FEA analysis results that were presented in the study was in the range of 2X of the Weibull analysis results. Burnette et al. noted that simulations indicated highest creep strain energy, but the failure analysis suggested all the failures on the PCB side. This proves that the material properties characterization plays a very important role in the FEA simulations. Table 5 will explain all the measured and predicted results and it will also present the multifaction factor for all the test conditions.

Epoxy	Predicted η (in cycles)	Measured η (in cycles)	Ratio Pred./Meas.
A	3690	2320	1.59
B	7390	5420	1.36
C	7630	5440	1.40
D	9470	>6000	n/a
none	6690	2490	2.69

Table 5: Predicted and measured values of characteristic life of five CBGA assemblies [21]

Hongbin Shi et al. Performed a study which has taken different underfill configurations into consideration. It is indicated that the No UF case has given highest TTF compared

to the fully and partially filled configurations [22]. The CTE of the material that was used in the study was 60 ppm/°C below T_g and 200ppm/°C above T_g . It is indicated that the Partially filled underfill worked better than the fully filled underfill condition. The T_g of the material that was selected is low (85°C). Figure 4 will represent the Weibull analysis results that was presented for all the configurations. This reduction in the characteristic life was contradicting the previous case with the increase in the characteristic life.

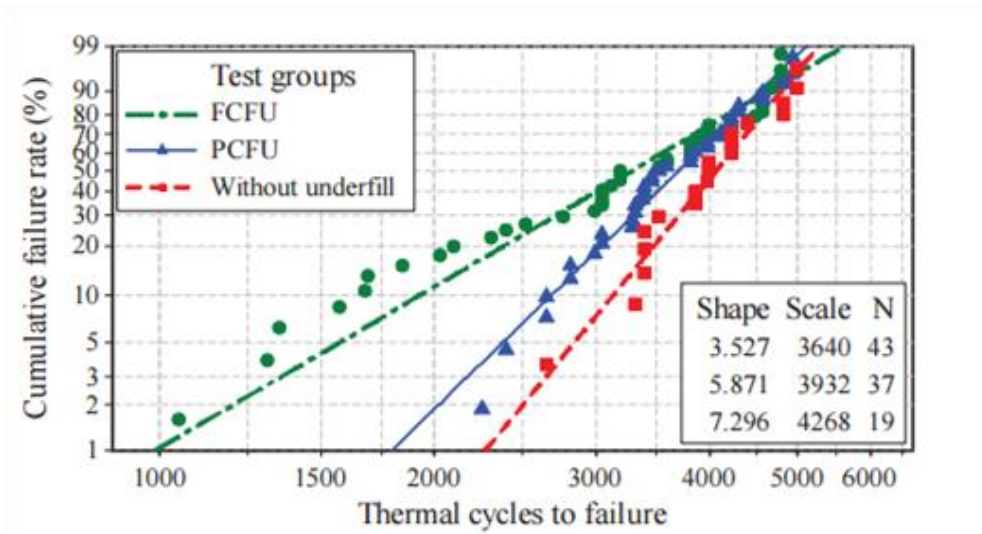


Figure 4: Weibull analysis results of the study for different configurations [22]

Shi et al. performed a study identical to the previous case by taking different configurations into consideration and indicated the reduction in the fatigue life of the packages with the underfill compared to the packages without underfill. Thermal cycling was done from -40 to 125 °C and Table 6 will explain all the underfill properties and different configurations that were considered for the experiment. In this case also partially filled underfill condition worked better than the fully filled underfill condition [23]. The results of the test will be presented in table 7.

Underfill	Viscosity at 25°C (mPa.s)	T _g (°C)	CTE (ppm/°C)		Modulus (GPa)	Typical curing performance
			α1	α2		
A	375	69	52	188	3.080	8 minutes at 130°C
B	2000~4500	85	60	200	3.500	5 minutes at 120 °C

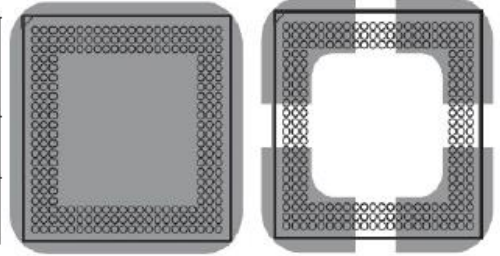


Table 6: Underfill properties and configurations (fully filled and corner bonding) [23]

Sample	FCFU-A	FCFU-B	PCFU-A	PCFU-B	Control
α or $N_{63.2\%}$	3206	3640	3406	3932	4268
$N_{10\%}$	2844	3281	3100	3694	4059
$N_{1\%}$	712	988	1046	1796	2272
$N_{\text{First failure}}$	960	1046	1519	2251	2650
β	3.056	3.527	3.895	5.871	7.296
# Failures /# Samples	41/45	43/45	39/45	37/45	19/45

Table 7: Weibull parameter estimates for thermal cycling experiment [23]

All the studies that has been done, the thermal cycling was only done from -40 to 125 °C, which is low for the high temperature applications. The T_g of the materials that were tested was also low and the CTE of the material was very high. It is mentioned in some studies that low CTE material will improve the reliability of the packages and in some studies, it is mentioned that the fatigue life decreased after the application of the underfill. In all studies that was performed previously there is some uncertainty about the performance of the underfills under thermal cycling and the studies that were performed is not providing any conclusive guidelines for the selection of the underfills for the high temperature applications.

This research was performed to check the reliability of the solder balls under a high T_g and low CTE materials combined with a different material property (modulus) that was neglected in the literature and to create a guideline for selecting the material for high temperature applications.

Experimental Setup

Background

All the commercially available underfills were selected and sorted according to the properties that were provided in the data sheets. Most of the commercially available underfills have $T_g < 150^\circ\text{C}$, Modulus $> 4\text{Gpa}$ and $\text{CTE} > 20\text{ppm}/^\circ\text{C}$. It was proved that the underfills with low CTE would perform better in a thermal cycle environment [15]. But most of the research till now was performed only on the low T_g materials and low thermal cycling conditions. It is very important verify the reliability of the solder joints

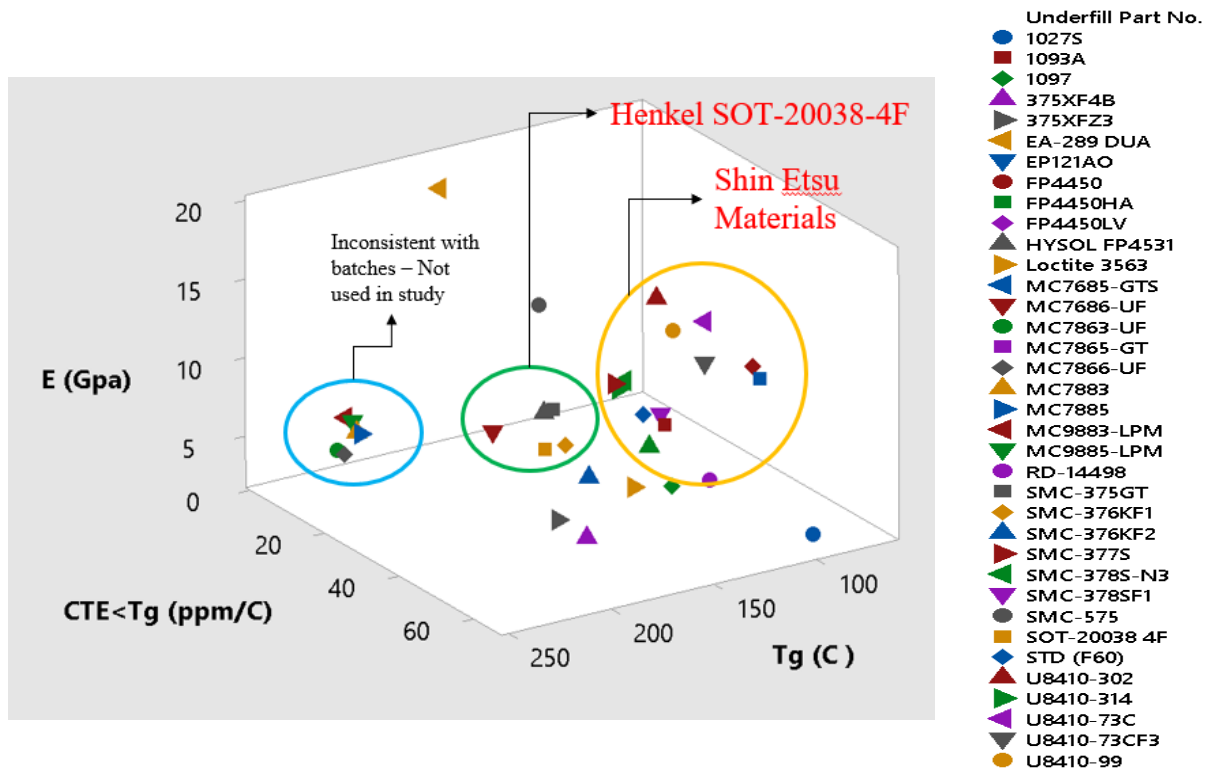


Figure 5: All the commercially available underfills in the industry

with underfill at high thermal cycle conditions. Three underfills were selected for different test configurations (corner bonding and fully filled) to see the reliability of the BGA packages under thermal cycling conditions. Figure 5 gives a 3D representation of all the commercially available underfills in the industry.

S. No.	Underfill	Type	Resin
1	MC7863-UF	One Part	Cyanate ester
2	MC7686-UF	One Part	Cyanate Ester
3	MC7866-UF	One Part	Cyanate Ester
4	Loctite 3563	One Part	Epoxy
5	HYSOL FP4531	One Part	Epoxy
6	EP121AO	Two Part	Epoxy
7	SOT-20038-4F	One Part	Epoxy
8	Protavic ANE 10932	One Part	Epoxy
9	Sanyu Rec-EZ471	One Part	Epoxy

Table 8: Resin in the underfills that were benchmarked

After benchmarking all the commercially available underfills, each major underfill group was grouped with respect to the chemical composition. Table 8 represents all the major underfills groups according to their chemical properties. In the experiment all the underfills that were selected are epoxies.

After benchmarking all the commercially available underfills, initial FEA analysis was performed to compare and select the underfills according to their properties that are available in the data sheets. FEA was performed on different underfill configurations (corner bonding, fully filled). In each case stresses on the solder balls were estimated with FEA and the cycles to failure was calculated with the empirical formulas (inelastic low cycle fatigue model) [24]. This section will only explain the preliminary FEA analysis results, detailed explanation of the FEA will be explained in the coming sections.

There are two configurations that were taken into consideration for the experimental studies (fully filled and corner bonding) Table 9 will explain all the corner bonded materials that were considered for initial FEA with the properties.

Corner Bond Material	Elastic Modulus (GPa)	CTE1 (ppm/C)	CTE2 (ppm/C)	T _g (C)	Viscosity (cps)
----------------------	-----------------------	--------------	--------------	--------------------	-----------------

AIT MC7686	>6	22	140	175	10000
DELO GE-765	9	18	60	185	22000
LORD ME-456	6	19	60	135	90K-150K
Structlite 8202	1.15	14.9	166.6	90	330
Polysciences	3.5	15	100*	150	20000
Master Bond EP121AO	4.1	21	149	135	55K-95K

Table 9: Properties of the corner bonded underfill materials used for preliminary FEA analysis

The material properties that were provided in the table was used for the FEA analysis and the initial FEA analysis that was done is only for the comparison purposes. All the FEA analysis was performed on the BGA 256 package. This package was selected randomly to verify the credibility of the FEA and for the selection of the underfill for the experimental studies. The initial FEA suggested that the AIT MC7686 with high T_g and low CTE1 will perform better, but because of its inconsistent properties and higher void content that was found in the preliminary characterization it was not selected. Lord is selected over structlit due to its name for the corner bonded underfill. All the results of the initial FEA analysis for the corner bonded configuration is presented in figure 6.

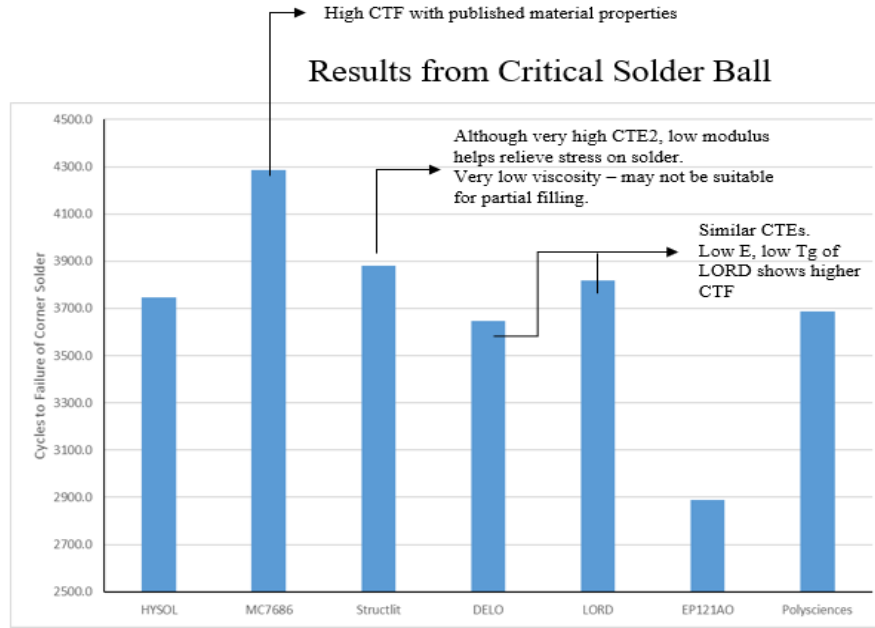


Figure 6: Results of the preliminary FEA analysis for the corner bonded materials

Lord material was selected in the corner bonded configuration. In the fully filled configuration all the materials were benchmarked and the combination of high and low values of the properties were taken for the preliminary FEA analysis to find the best possible underfills that were available in the industry for the experiment. The preliminary analysis was performed with a quarter symmetrical model and the critical solder ball was found to be on the end of the die shadow. All the materials that were tested was shown in the table 10.

Initial FEA analysis predicted that the Henkel material with moderate T_g , low CTE and moderate modulus will perform better. The next best material that was found is the Shin Etsu, but the T_g of the material was too low and the reliability of the solder balls with the high T_g material was not yet proven. So, a different material was chosen to see the reliability of the solder balls when the underfill has high T_g and high modulus.

Standard Underfill Materials								
T _g	CTE	E	Manufacturer	Product	T _g (C)	CTE1 (ppm/C)	CTE2 (ppm/C)	E (GPa)
L	L	L	Henkel	Loctite 3563	130	35	110	2.8
L	H	L	Sun STAR	1027S	90	64	163	2.7
L	H	H	Namics	U8410-73C	88	31	95	11.5
H	L	L	AIT	7686	175	22	141	6
H	L	H	HYSOL	FP4531	144	30	100	7.6
H	H	L	Shin Etsu	375XF4B	189	55	122	4.2
H	H	H	Shin Etsu	375GT	160	30	97	8
H	L	L	Henkel	SOT-20038-4F	155	25	58	4.6
L	L	H	Shin Etsu	SMC 575	140	15	65	12
L	L	H	Shin Etsu	SMC-356 SDL-4	140	26	95	8
H	L	H	Sanyu	EZ-471-3	196	23	56	9.4

Table 10: Properties of the fully filled underfill materials used for preliminary FEA analysis

Figure 7 will explain all the preliminary FEA analysis results of the fully filled underfill.

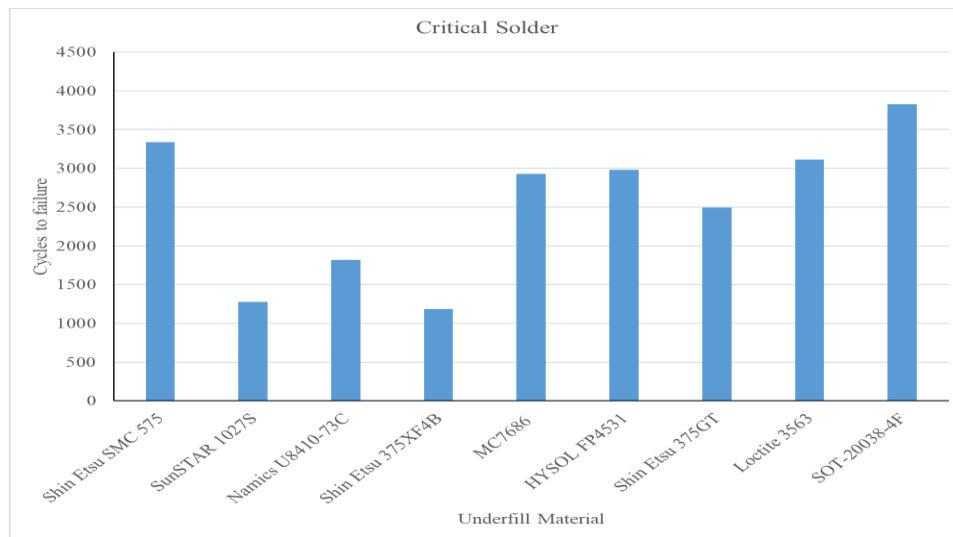


Figure 7: Results of the preliminary FEA analysis for the fully filled underfill materials

Preliminary FEA analysis predicted that the material with high T_g, Low CTE and high modulus will perform better and then the Henkel material with all the moderate

properties and then the corner bonded material and the least TTF was predicted for the No UF case. The No UF case was selected for the reference purposes. The results of the preliminary FEA for all the configurations is presented in figure 8.

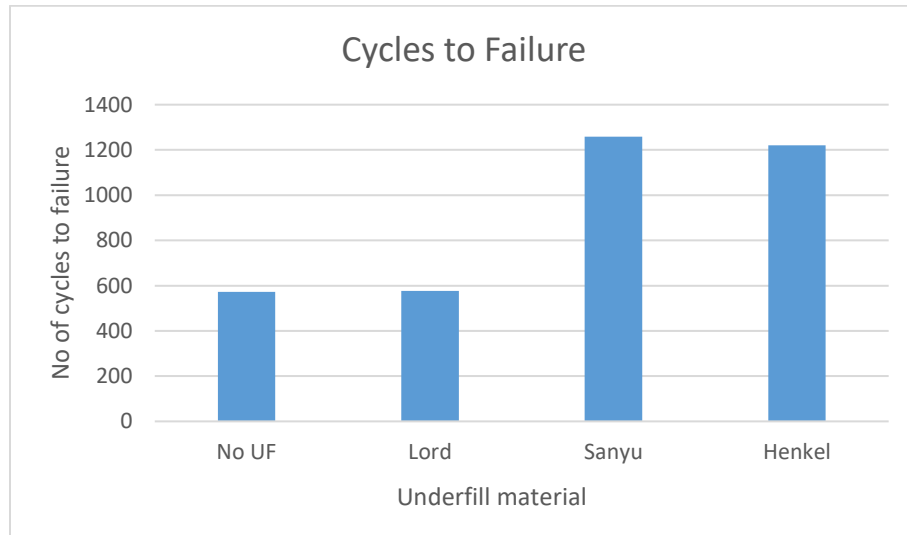


Figure 8: Preliminary FEA analysis prediction of all the material that were selected for the experiment

This FEA analysis was performed on the BGA 256 package and FEA was done only for the comparison purposes.

Design of Experiment

After the completion of the initial characterization and FEA. The DOE plays a vital role in the collection and validation of the data. Different designs were taken into

consideration. Each design is varied with the types of devices and number of devices on the board. Data should be collected for different stress conditions in an experimentation so that the research can be generalized. Different types of devices were taken into consideration for the experiment and they were configured as shown in figure 9. After taking the requirement and variability into consideration design H was considered for the experimentation.

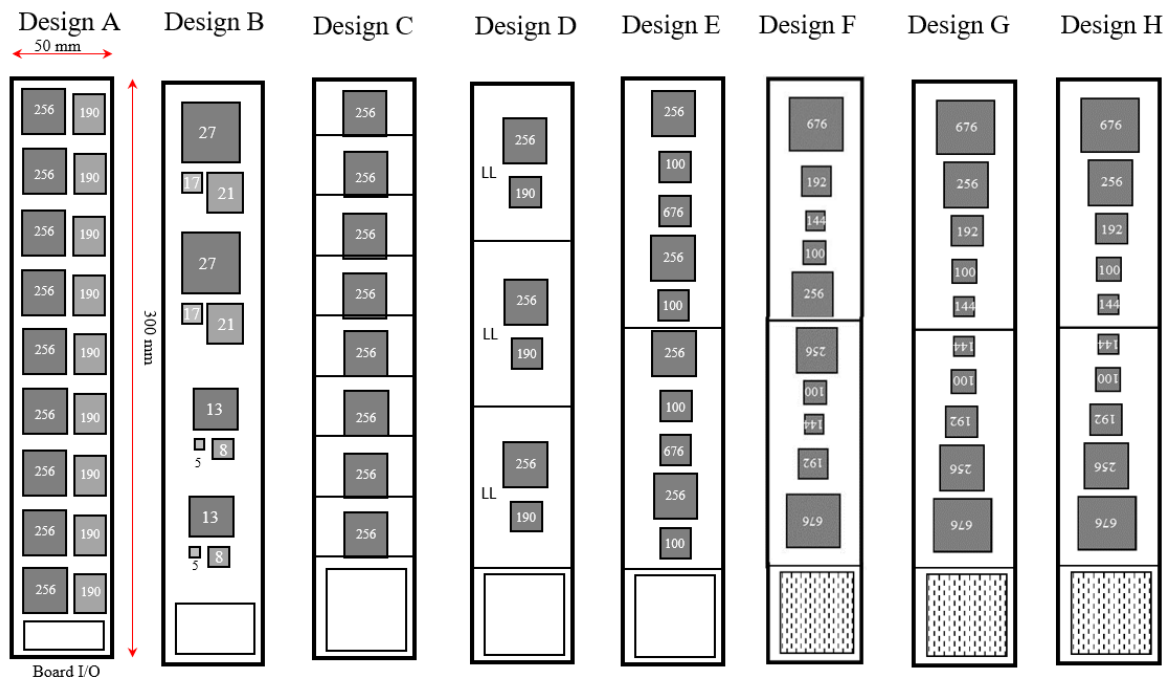


Figure 9: Designs of different boards with packages that were considered for the experiment

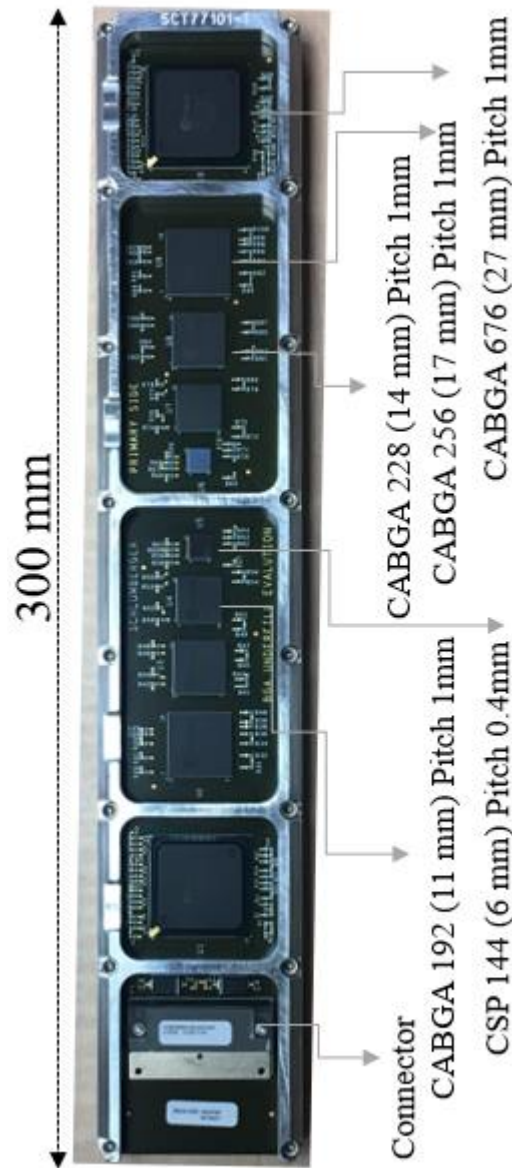


Figure 10: Final design of the board with components that was used in the experimentation

Five different types of BGA packages with varying sizes from large to small was selected and the two packages of each type which is a total of ten packages on the board as shown in figure 10. Three different types of underfills were selected with five different kinds of BGA packages for each board. A total of 11 board were designed for the accelerated thermal cycling testing. All the boards were subjected to a thermal

cycling condition from -40 to 185°C. Each component will experience these thermo mechanical stresses and the components will be monitored for getting the TTF data.

Table 11 explains the test vehicle for the experiment.

Temperature Cycling (-40 to 185°C)		
		No. of Boards
	No UF	1
Fully Filled	Henkel SOT 20038-4F	4
	Sanyu Rec EZ-471-3	4
Corner Bonded	Lord ME-456	2
	Total	11

Table 11: Number of boards of each underfill that was used for the experimentation

Test Vehicle

Performance of the electrical characterization to monitor the in-situ data is challenging in a highly populated board. Each device has an average of three daisy chains to monitor. Each daisy chain requires 2 I/O's for a two-wire measurement and 4 I/O's for the 4-wire measurement, which makes the total number of I/O's count as 60 and 120 respectively. This is not feasible in a highly populated experiment monitoring.

The team at SLB came up with the voltage monitoring method. It requires only 37 I/O's per board for the in-situ monitoring through isolation and continuous power supply. Current will be passed through the solder balls for checking the continuity. This was done with the help of a power supply of 2.5V and 2.5mA. All the daisy chains on the

board were monitored with the help of the data logger for the voltage. Discontinuity will be found if there is a change in the voltage.

As shown in the figure 11 in 37 I/O's 32 are allotted for the daisy chains which were split between 10 different devices, 2 are for the power input and return and 1 is for the ground. This is the split of all the I/O's on the board. This is a voltage divider testing scheme. Each daisy chain consists of 90-100 solder balls. Change in the voltage is considered as failure. Resistors will split off for every 30 solder balls and failure in the solder ball will bring the change in the voltage divider resulting in change of voltage. With the change in the voltage the failure across the resistor split can be determined, which is mentioned in the table 11.

- 2 – Power
- 2 – Power return
- 1 – Common ground
- 32 – Daisy chains – Split for 10 devices

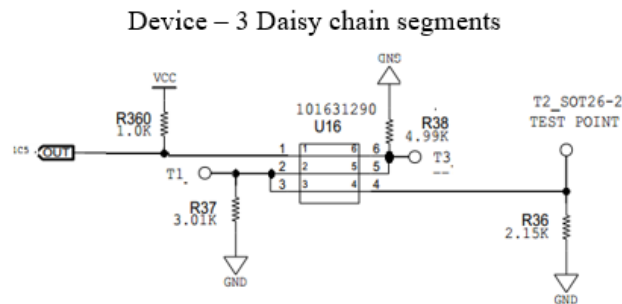


Figure 11: Circuit diagram of the resistors that was present on the board that was used for 1 wire measurement

All the solder balls were not accessible at the bottom of the board for the testing purposes. The test points were set accordingly after every 30 solder balls. Each test point was readily available at the bottom of the board for the manual electrical testing. Different test cases were defined for locating the failures manually. There is a chance for the failure of the resistors. This case was predefined in the experiment as shown in

the table 12. The in-situ monitoring will give the data about the different types of packages in the thermal cycling test.

Test Information		
Situation	Value	5V VCC
Good	1/2 VCC	2.502824
U16(2,5) Bad	5/6 VCC	4.165275
U16(3,4) R36 Bad	2/3 VCC	3.262373
U16(1,6) Bad	VCC	
R37 Bad	0.6 VCC	3.002071
Manual Test T3 to determine		
R38 Bad	0.56 VCC	2.781885
Manual Test T2 to determine		
R36 Bad	2/3 VCC	3.262373
U16(3,4) Bad	0V	

Table 12: Definition of the failure with the change in the voltage values

Environmental Testing

Accelerated life testing was conducted in the environmental chamber at one of the labs in CALCE. Each component was subjected to a thermal cycling condition of -40 to 185°C. Negative temperatures were regulated by the liquid nitrogen tanks. This thermal cycling condition was selected to imitate the real-life conditions of the down hole applications. Thermal cycling profile was shown in figure 12.

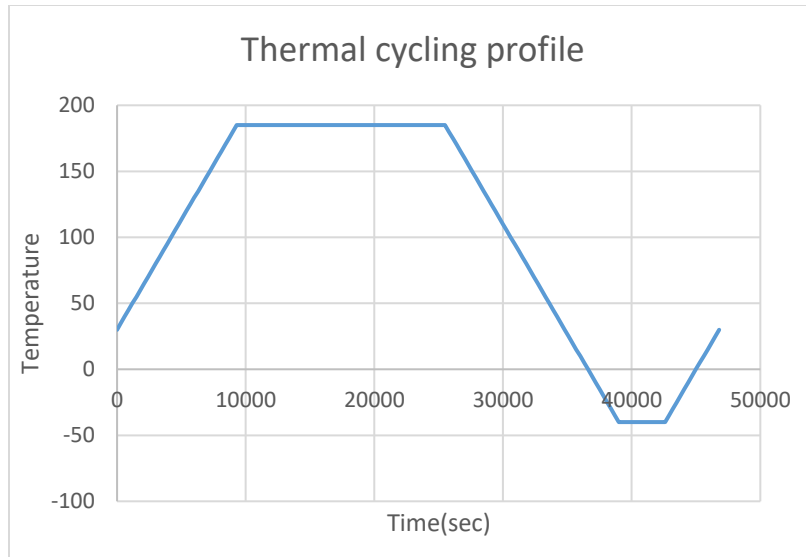


Figure 12: Thermal cycling profile used in the experiment

For the accelerated life testing, experiment was started with 11 test boards inside the chamber as shown in figure 13 and each test board was named and monitored for the voltage change continuously to find the first TTF of the components under the thermal cycling conditions. There are three thermocouples attached to the three boards as shown in the figure 13 to continuously monitor the temperature of the boards. All the three thermo couples were calibrated and the data that was collected from the in-situ monitoring and used in the data analysis for finding the TTF of the BGA packages.

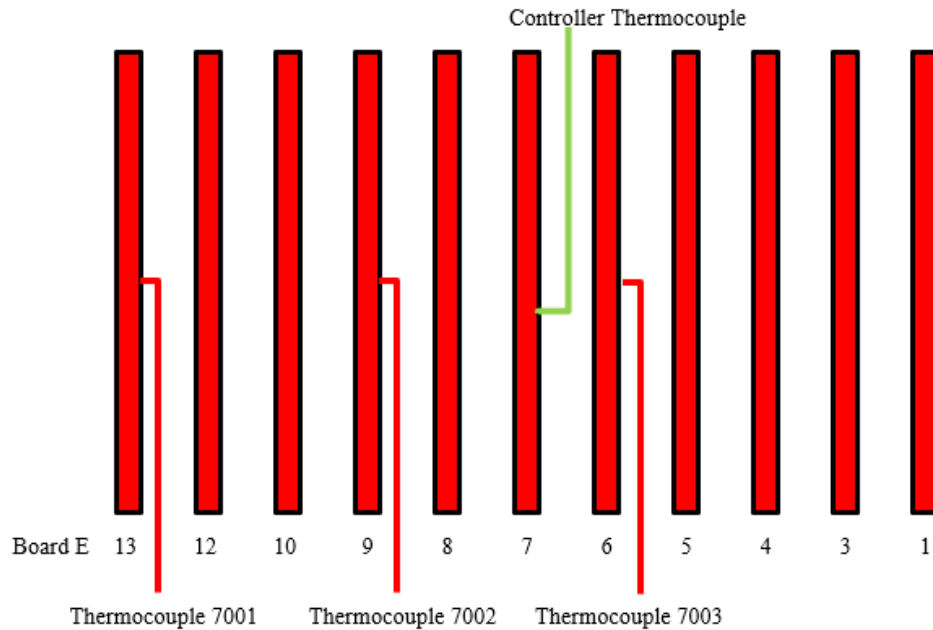


Figure 13: Arrangement of the boards in the environmental chamber with all the thermocouple

The thermal cycling profile was selected in such a way that it will not input any additional failure modes and mechanisms. The ramp rate was given 1°C/min and the test was started at room temperature, it will reach the highest temperature of 185°C and the dwell time at 185°C is 4.5 hours. The ramp down rate is the same and it will cross the room temperature and will reach the lowest temperature of -40°C. The dwell time at lowest temperature is 1 hour. After completion it will reach the room temperature. The time taken to complete a full cycle is around 13 hours. Data was collected for every two weeks and the liquid nitrogen tank were continuously changed to provide the cooling.

Data Analysis

Data was collected for every 2 weeks and is analyzed for any new first failures. The data that was collected will be analyzed for the TTF and was plotted in a Weibull chart to compare the different underfills.

Data was collected with the help of Keysight data logger. Data that was collected was exported to the excel sheet and each channel was separately analyzed for the change in the voltage with the temperature cycle.

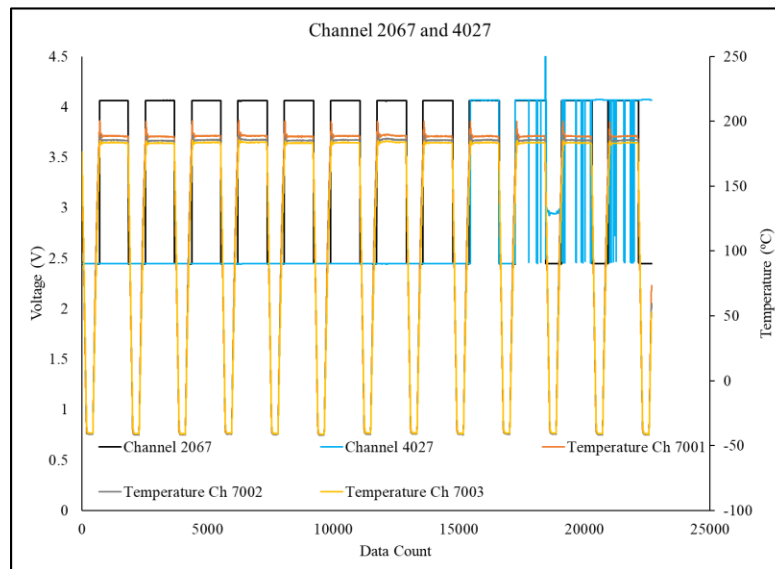


Figure 14: Identification of the failure from the in-situ monitoring data and comparison between the three thermocouples

Figure 14 shows the basic analysis method that was taken to find the TTF of the first component failure. All the data was converted into a graph, voltage and temperature were plotted in two different axes. When there is a change in voltage reading for a channel, it was considered as failure. In the figure 14 the blue line is the reading of the voltage for the channel 4027, after few thermal cycles the voltage reading varied suggesting the failure on that thermal cycle. Total number of thermal cycles were

counted to that point and with the help of data that is available the first TTF of the component was determined. All the first TTF of the components were noted and used for the Weibull analysis. First TTF data is presented in table 13. The gradient in the thermal chamber was verified with the help of the thermo couples. They were set along with the boards to measure the temperature continuously. The three channels that were mentioned in the figure 14 7001, 7002 and 7003 represent the thermocouples and the difference in values between the thermocouples is very small. This proves that the temperature gradient is negligible when we compare it between the outermost corner boards in the experiment.

No UF				
BGA	BGA	BGA	BGA	CSP
676	256	192	228	144
357	60	256	80	51
	151	285	95	60

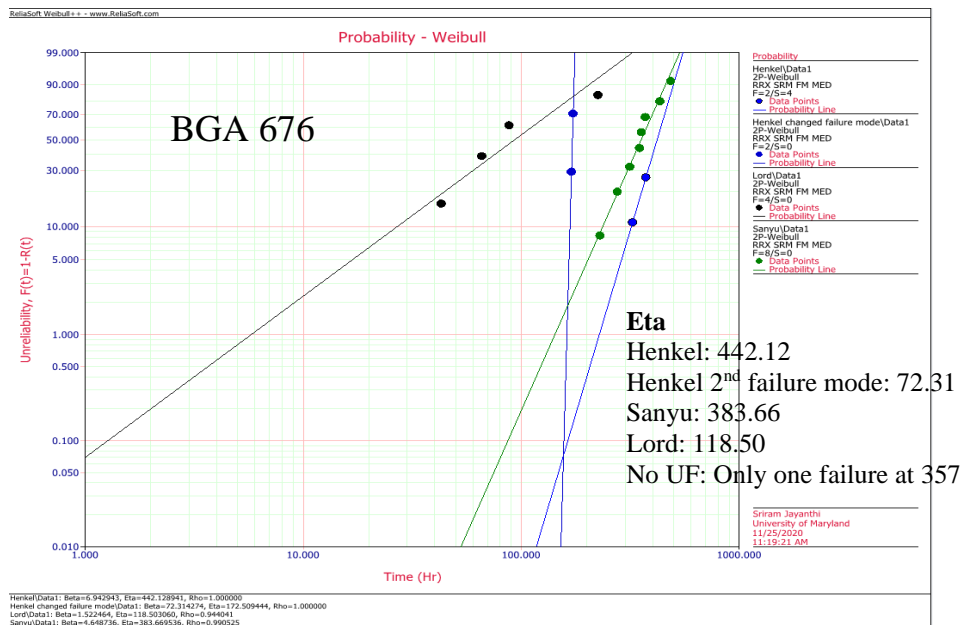
LORD ME-456				
BGA	BGA	BGA	BGA	CSP
676	256	192	228	144
43	21	46	324	153
66	32	48		184
88	36	60		321
225	36	69		

HENKEL SOT 20038-4F				
BGA	BGA	BGA	BGA	CSP
676	256	192	228	144
170	110	179	478	297
173	209	213	480	
315	296	287	484	
324		316		
373		354		

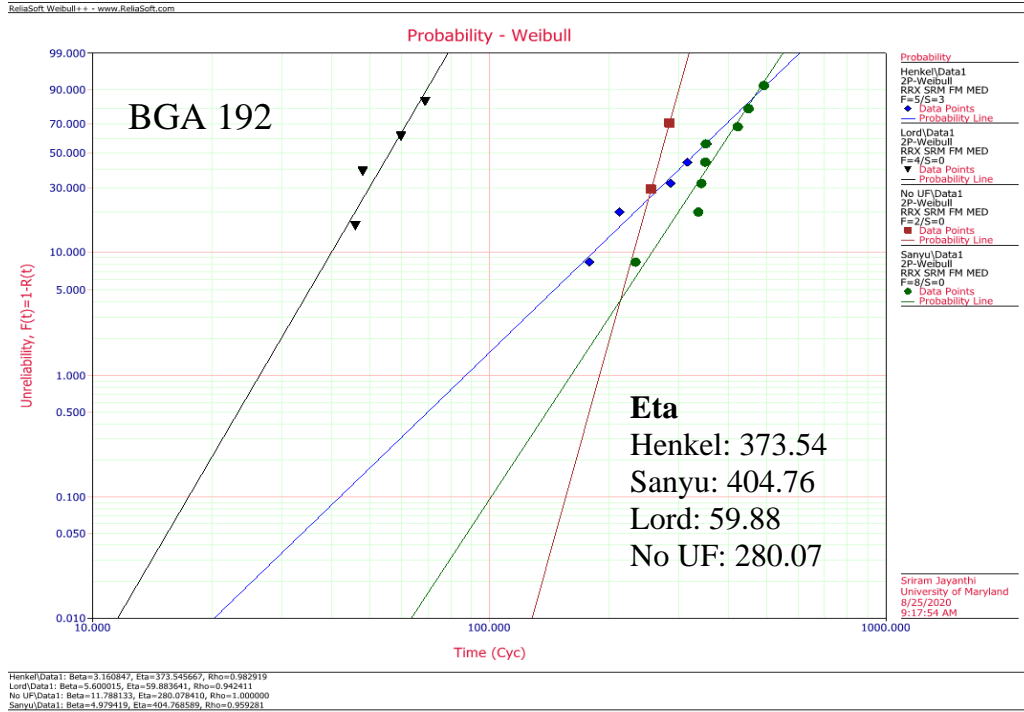
SANYU REC EZ-471-3				
BGA	BGA	BGA	BGA	CSP
676	256	192	228	144
230	135	234	354	196
276	185	337	373	275
315	193	351	434	276
356	240	343	430	288
349	277	352	418	315
371	277	451	483	338
433	315	424	501	389
485	368	493		321

Table 13: First TTF of each component that was collected from the in-situ monitoring

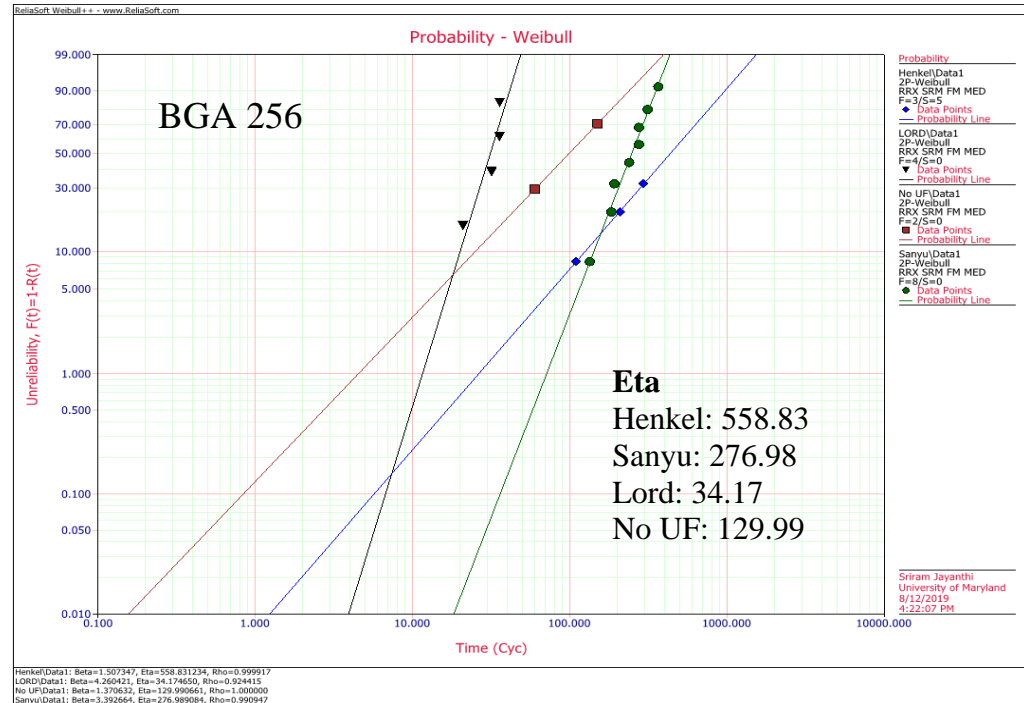
After getting all the data about the TTF of each component on the board a Weibull analysis plot was generated for comparing different underfills. Weibull analysis was taken with different components types on the board. All the analysis that was done is for the comparison purposes only and to find the failure mechanism shifts in the packages after some amount of thermal cycling.



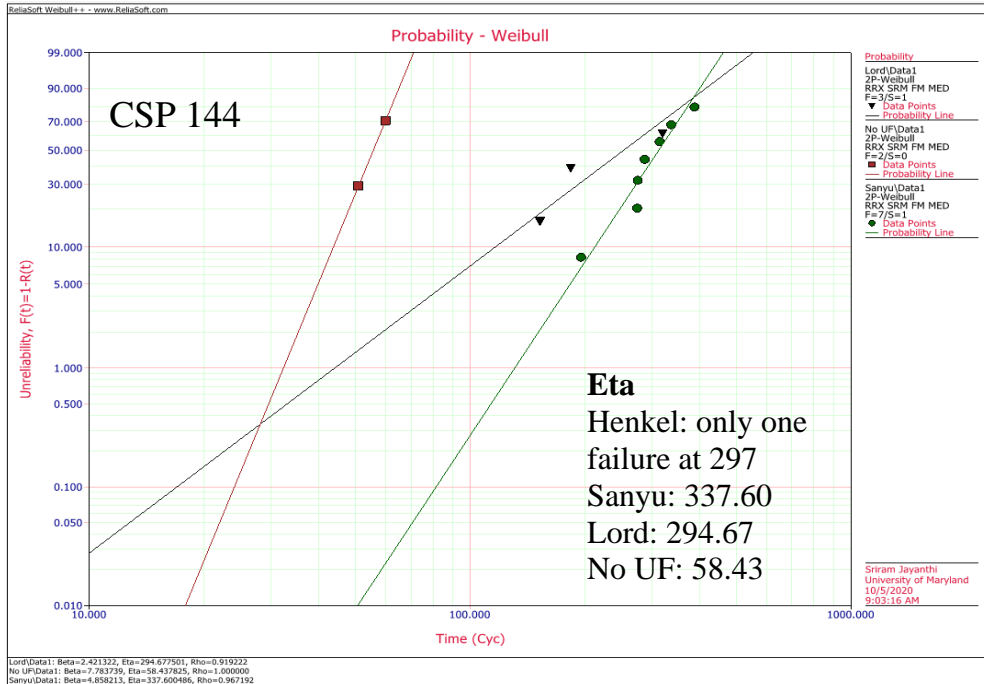
(a)



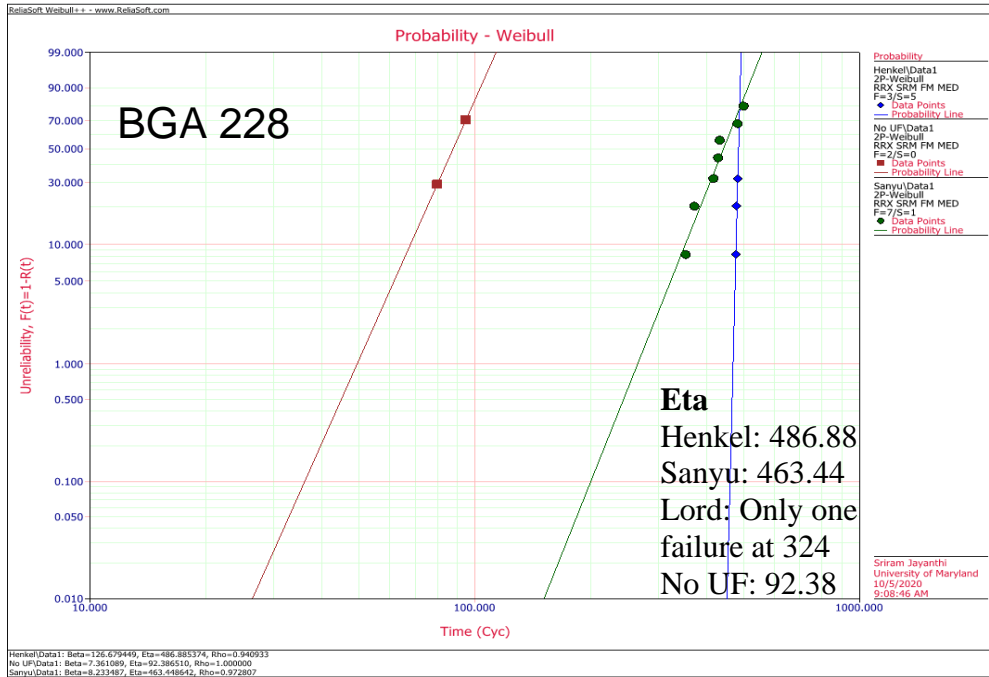
(b)



(c)



(d)



(e)

Figure 15: Weibull analysis results of all the components that went through thermal cycling test

From the Weibull analysis results shown in Figure 15, Henkel material with moderate material properties performed better than all other underfills for all the packages except for BGA 192. This uncertainty can be attributed to the difference in the constraints near the BGA 192 package. This hypothesis should be verified with further FEA analysis. The Henkel material packages (BGA 676 & BGA 192) showed early failures, Resulting in the lower TTF in the start. As the experiment progresses the failure rate of the components with Henkel decreased resulting in higher TTF of the components. The reason for the early failure will be explained in the failure analysis section. The Sanyu material components performed better in the start of the experiment, but as the experiment progresses there is a shift in failure mechanism in the components resulting in the lower TTF at the end of the experiment. The change in the failure mechanism may be due to the material decomposition or change in the material properties with aging, which will be explained in the coming sections. Lord performed worst for most of the packages. Although the corner bonded material reduces significant warpage stresses that are acting on the components it may have exerted more stresses on the corner solder balls resulting in the early failures of the packages. These lord boards were taken out early for the failure analysis to see the exact failure mechanisms that might be occurring in the package. No-UF board components performed better than the lord material in some cases, but it is only taken for the reference purposes. Some UF components were not presented in the Weibull analysis because of the lack of failures in the experiment. In case of No-UF and Lord components there are not enough components for the testing and to see the exact failure mechanisms both those boards were taken out early in the testing. They can't be compared to the fully filled underfills.

But both the fully filled UF boards were taken out at the same time to make the comparison between them possible. Preliminary FEA analysis predicted that Sanyu material with High T_g , low CTE and high modulus would perform better than the Henkel material with all the moderate properties.

Due to all uncertainties that were presented in the Weibull analysis, a failure analysis was performed to understand the reasons for these uncertainties. Before going to the failure analysis, the verification of the FEA is important, all the FEA results were verified with the help of probing which will be explained in the next section.

ANOVA Analysis

An additional ANOVA analysis was performed to verify the difference between the means of the two groups. In this analysis an assumption was taken at the start i.e. the means of the two groups were same at the start of the analysis. After the analysis it was proven that there is difference between the means of the groups that were taken. The ANOVA analysis will consider a normal distribution which won't correctly represent the failure rate that was happening in the experiment, so this analysis was only considered for the comparison purposes and for the rest of the document all the results were discussed from the Weibull analysis. BGA 256 component was considered for this analysis. Suspended data was assumed as the component failed at the end of the experiment. Table 14 represents all the data that was considered for the analysis.

Henkel	Sanyu	Lord	No Underfill
--------	-------	------	--------------

110	135	21	60
209	185	32	151
296	193	36	
514	240	36	
514	277		
514	277		
514	315		
514	368		

Table 14: Data considered for the ANOVA Analysis

Groups	Count	Sum	Average
Henkel	8	3185	398.125
Sanyu	8	1990	248.75
Lord	4	125	31.25
No Underfill	2	211	105.5

Table 15: Results of the Analysis for different Underfill Materials

ANOVA						
Source of Variation	SS	df	MS	F	P-value	F crit
Between Groups	408701.9	3	136234	10.17373	0.000383	3.159908
Within Groups	241033.6	18	13390.76			
Total	649735.5	21				

Table 16: Results of the ANOVA Analysis

Henkel material is showing highest cycles to failure from the ANOVA analysis. In the Analysis it was proven that there is difference between the means of all the underfills. The low P value suggests that the initial assumption that is taken was wrong and the ANOVA analysis was significant. All the results of the ANOVA analysis were presented in Tables 15, 16. The graphical representation of the time to failures was presented in figure 16.

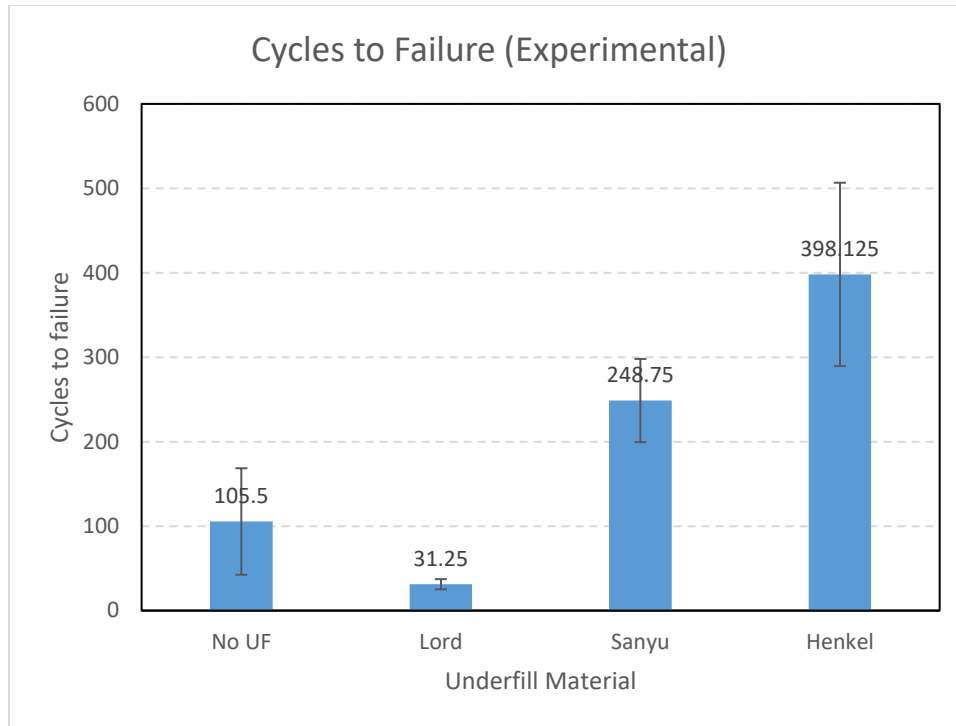


Figure 16: Graphical representation of the results with 95% C.I

Finite Element Analysis

A model was created in the Solidworks and was imported into the ANSYS Workbench to perform the thermo mechanical analysis on the BGA package with the underfills. Figure 17 will represent the FEA model that was used for the analysis. In Solidworks each and every component of the package was precisely modelled by taking the dimensions from the cross sections and most of the material properties were taken from the ANSYS library, except for the underfill properties which were characterized using the TMA and DMA. Linear behavior of the materials was assumed in the simulation except for the SAC 305, where nonlinear properties were assumed.[25,26,27]

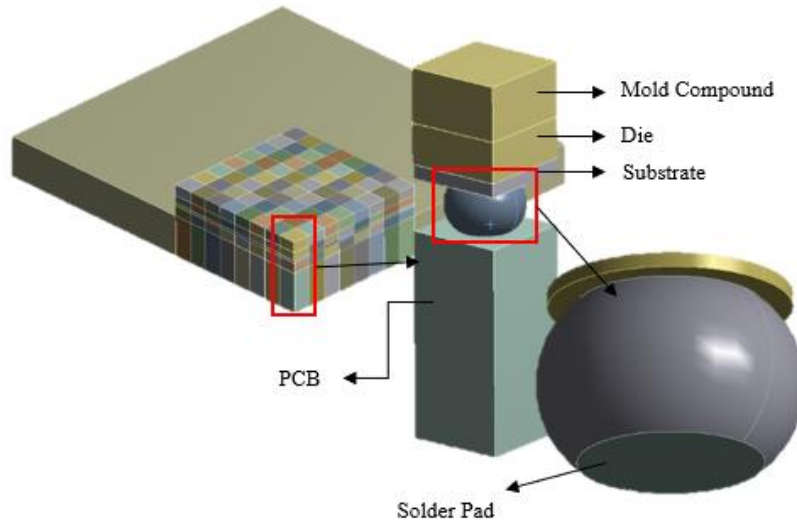


Figure 17: Depiction of the quarter symmetrical model with cut sections and the copper pads

Quarter symmetrical model was selected for the No UF case and the warpage was included for the packages with underfill to verify the FEA and the experimental results. Two sides of the quarter symmetrical model were given a symmetrical boundary condition and the package was subjected to a thermal cycling condition from -40 to 185 °C. Figure 18 will explain the boundary conditions that were taken for the FEA.

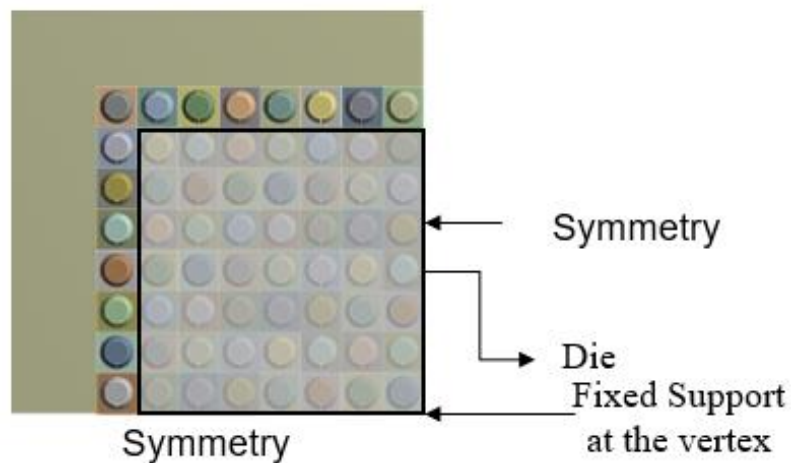


Figure 18: Boundary conditions that were applied to the quarter symmetrical model

After creating the model plastic work of the solder ball over the cycles were taken into consideration for finding the critical solder ball in the BGA package. In the No UF case the solder ball experiencing the maximum amount of stresses is the corner most solder ball from the neutral point, this can be attributed to the shear stresses that will be acting on the solder balls as the DNP increases. These shear stresses will act due to the combination of local CTE mismatches and the warpage. It was found through probing that most of the failures were concentrated on the outer chains of the packages. The failure mechanisms in the No UF will be explained in failure analysis. Figure 19 will explain the plastic work accumulated on the solder balls after thermal cycling.

The FEA model was verified with the experimental results and are matching well. In case of the No UF FEA predicted that most of the failures will occur on the outer chains of the package. All the packages were probed to find out the failure locations, most of the first failures were occurred on the outer chains of the BGA packages. All the packages were not taken out after the first failure in the board due to the different components that are present on the board and the different failure times for each package. Figure 20 will explain the failures in the packages of the No UF board after probing. The additional failures on the inner chains can be attributed to the warpage stresses that were acting at the time of thermal cycling.

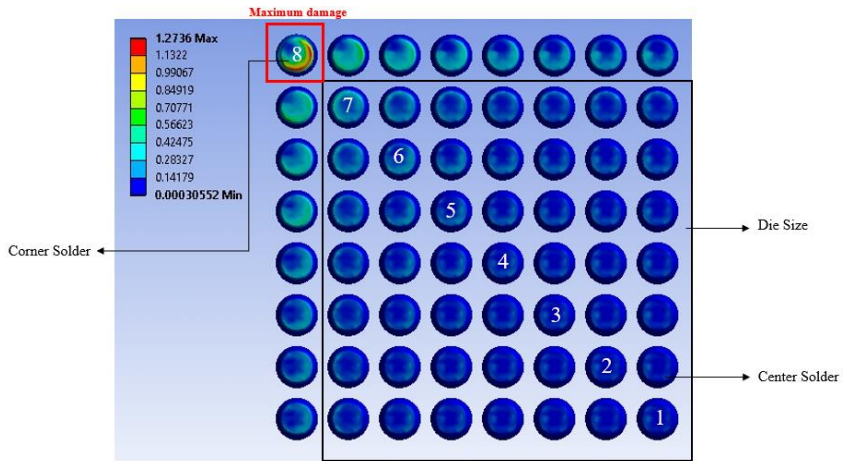
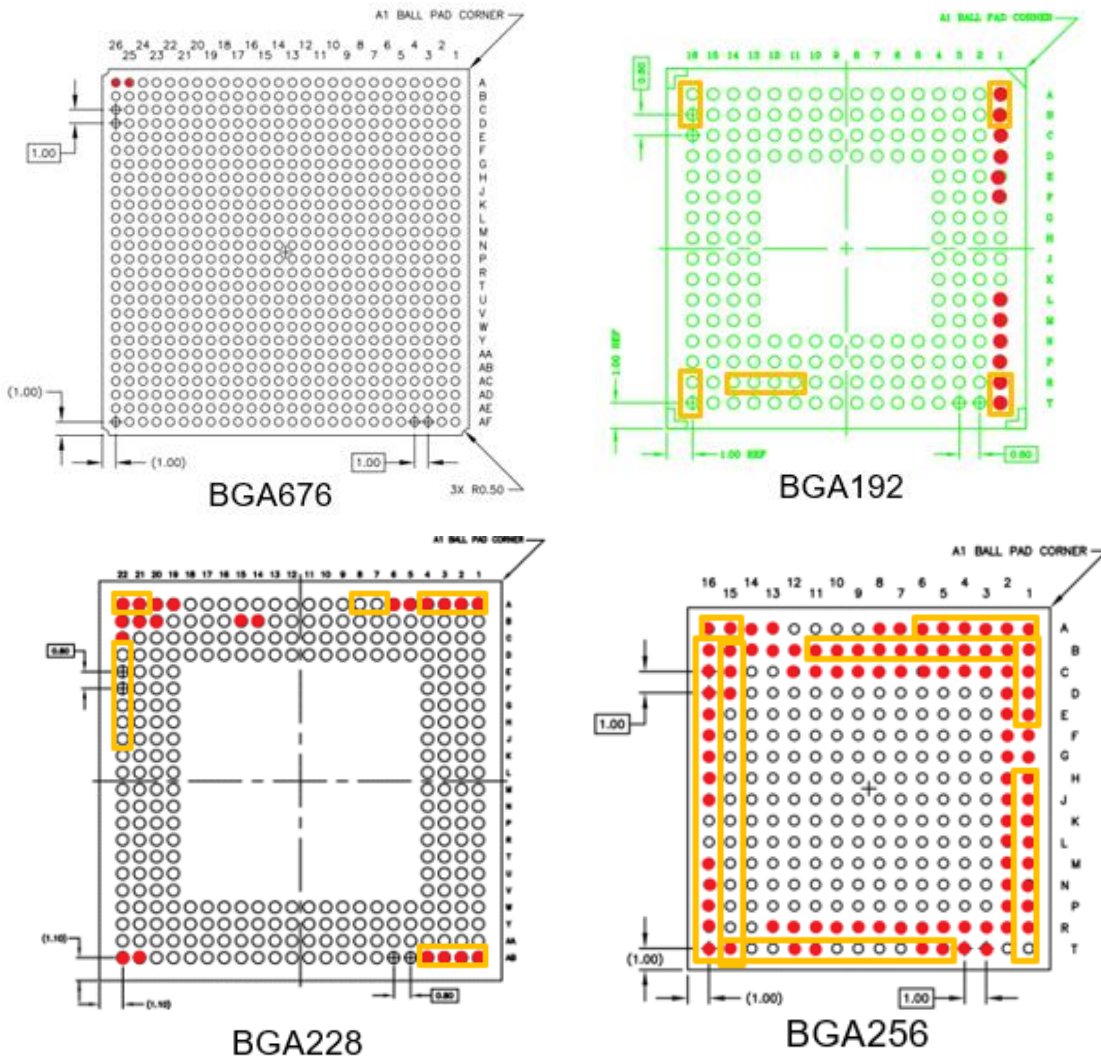
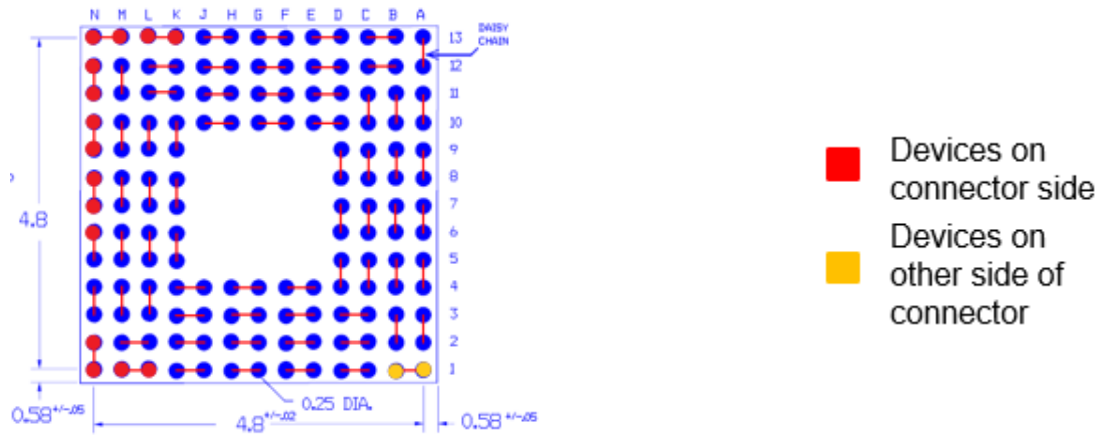


Figure 19: Plastic work across the solder balls for the No UF condition





CSP 144

Figure 20: Failure in the BGA packages found through probing for the boards without UF

The Preliminary FEA from the UF case doesn't match with the experimental results, to find the reason for the uncertainty a new FEA model was created by taking warpage of the board into consideration. A middle section of the board was created with the frame and the boundary conditions were given accordingly. Figure 21 will explain all the boundary conditions and the model. Figure 21 shows half symmetrical model of the BGA 256 package with the frame and the symmetry was given on the inner side of the board as shown in the figure b. All the inner faces of the holes on the frame were given fixed supports to replicate the original conditions, which is shown in figure c.

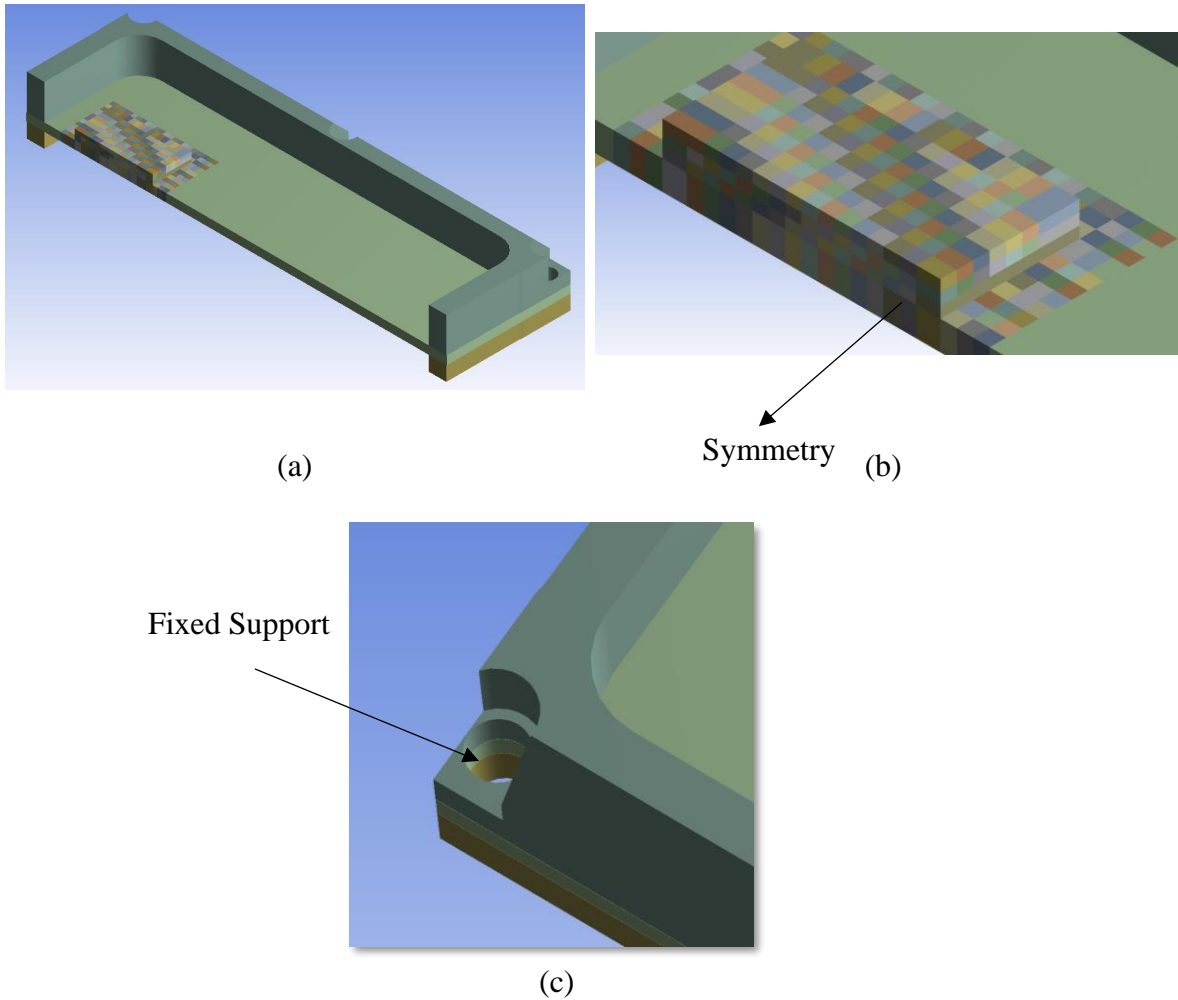


Figure 21: Half symmetrical model created for the UF case to include the warpage stresses

In the model with the warpage the corner most solder ball of the BGA package was experiencing the maximum amount of stresses, this can be attributed to the warpage stresses that were acted on the solder balls due to the board when it is subjected to high temperature. The plastic work of the solder balls is explained in the figure 22.

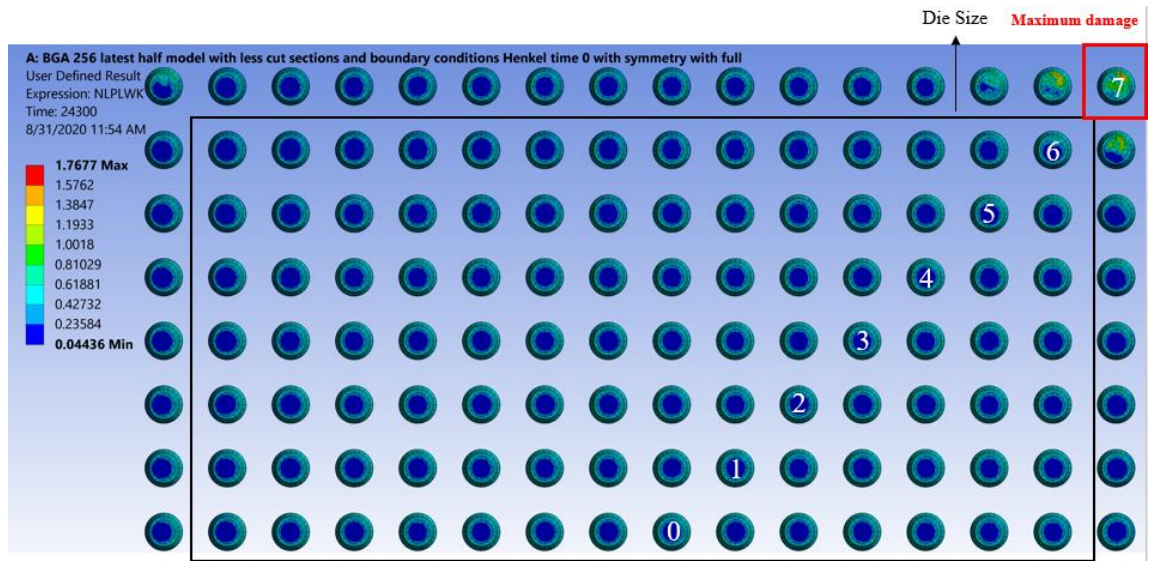


Figure 22: Plastic work across the solder balls in a UF board with the warpage stresses

The failures in the solder balls that was found through probing was verified with the FEA and they were matching well. Most of the failures that were found in the BGA packages were on the outer chains. The failures on the inner chains can be attributed to the warpage stresses that were acting on the solder balls after the first failure occurred. Figure 23 will explain all the failures that were found in the BGA packages after probing.

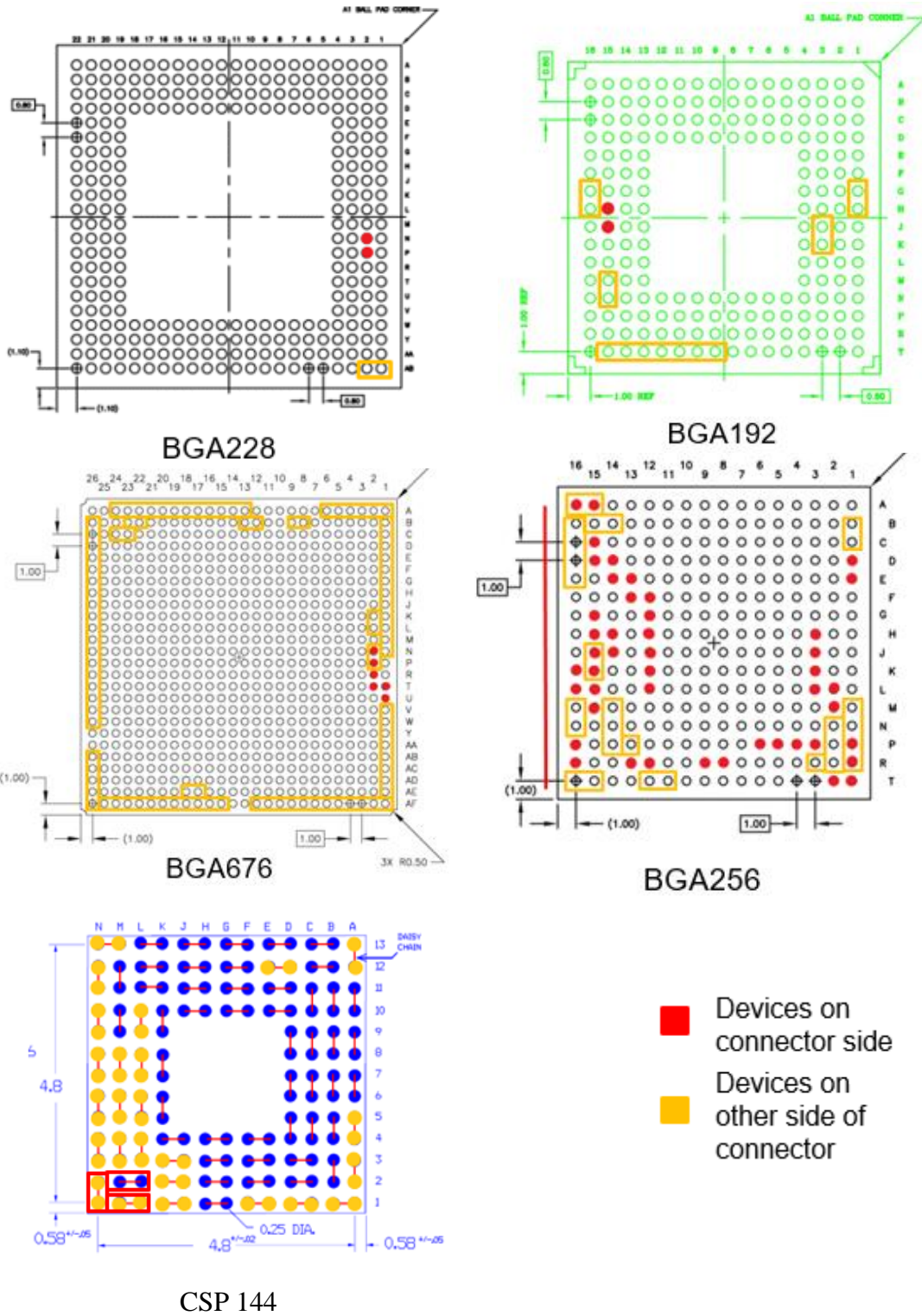


Figure 23: Failures in the BGA packages found through probing for the boards with UF

Failure Analysis

Failure analysis is an important method to find out the failure modes and mechanisms in a component or device when it is subjected to stress conditions during its life cycle. After finding the TTF of the components from the experiment the next step is to find the modes and mechanisms. To find the failure modes and mechanisms, location of the failure plays an important role. To locate the failure location a nondestructive analysis called probing was chosen.

Non-Destructive Analysis

It is a type of analysis where there won't be any damage to the components that are being tested. This analysis will give an insight on the location of the failures and it can also be used to find the void percentage in the underfill material filled under the BGA package. To find the location of the failure a probing approach was taken. A multimeter was used to check the continuity between the different solder balls. Current will be passed through the solder balls and checked for continuity. If there is continuity, then there is no failure and vice versa. All the components were divided into different daisy chains and each daisy chain was monitored for the change in the voltage. Through the in-situ monitoring, the daisy chains which has the failures are clearly known. With this information all the components were narrowed down and checked for the continuity between the solder balls. These steps were followed while performing the probing test.

1. Multimeter was set for performing the continuity test.
2. All the test points were located for each device and noted accordingly.

3. Probes were kept on two test points to check the continuity of the solder ball between the two test points.
4. All the solder balls were internally connected, the failure location was found if the current is not passing in between the two test points.
5. After locating the failure location with help of test points each solder ball was checked for locating the precise location of the failure.

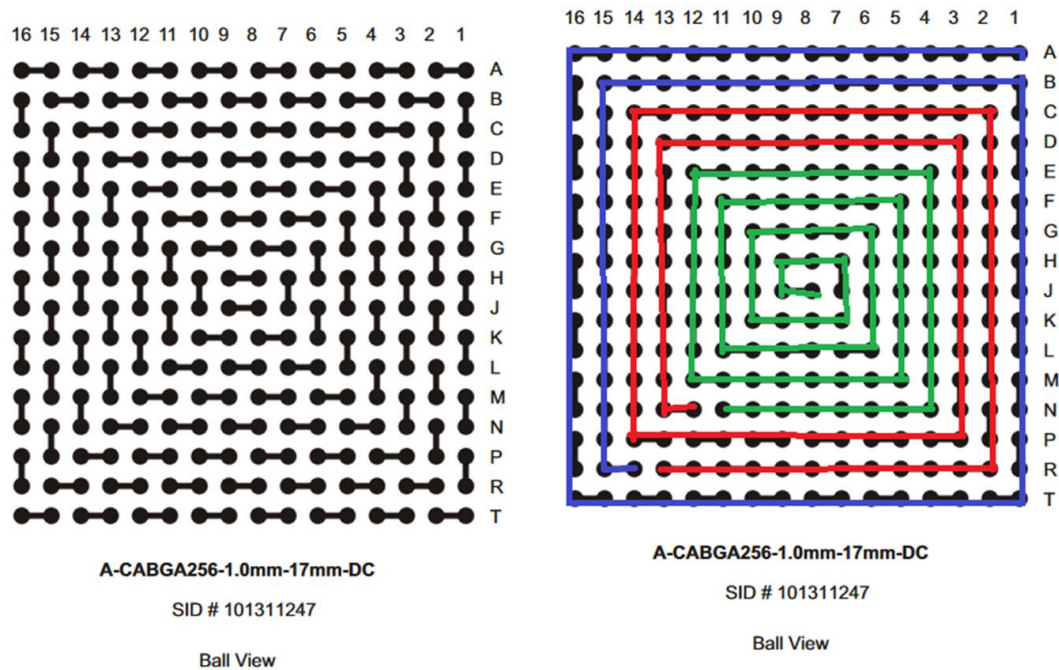


Figure 24: Graphical representation of the connections between the solder balls and the daisy chains in the BGA packages

In the BGA component as shown in the figure 24 two solder balls were connected externally for the testing purposes, if there is discontinuity while probing then there is a possibility that either one of the solder balls failed between the two solder balls that showed discontinuity.

The discontinuity between the solder balls suggest the failure locations in the package as mentioned in the figure 25. Probing analysis will also help with destructive analysis by discovering the direction through which the cross-sectioning should be done. In the figure 25 the lines are the daisy chains and orange dots are the failure locations that were found during probing.

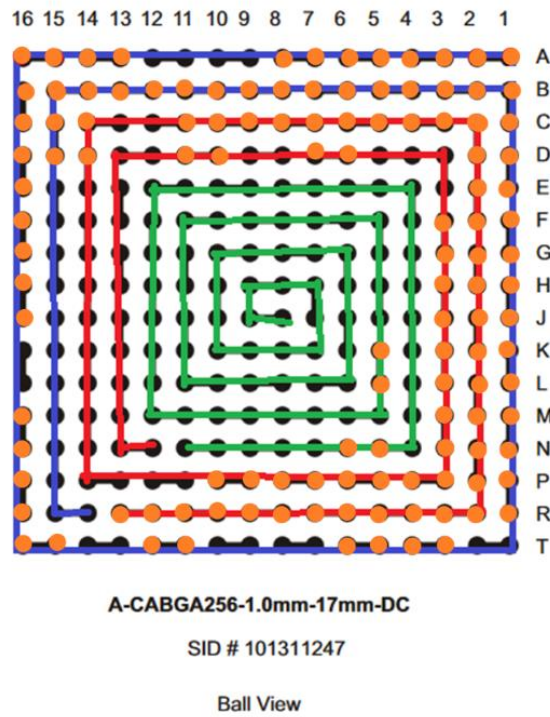


Figure 25: Failures found in the package with probing after the experiment

Destructive Analysis

To find the failure mode and mechanism, a cross sectional analysis was performed to discover the failure site by grinding through the solder balls. Each component was grinded towards the center of the solder ball where maximum information can be extracted. There are following processes involved in the destructive analysis.

All the boards that are removed from the testing went through the probing process. The next step after probing is the destructive analysis.

1. All the frames of the test boards were removed.
2. All the components of the board were potted initially before detaching the components from the board. This process is done to reduce the vibrational stresses that will be acting on the components while detaching the components from the board.
3. All the components were detached from the board with the help of a diamond saw.
4. After cutting all the components were cleaned to remove the extra dust particles and the components were potted in a cylindrical base with 8 hours cure epoxy resin and hardener.
5. All the components were grinded with the help of the grid sizes varying from 240 to 1200 grit size, where 240 is coarse and 1200 is fine grit paper.
6. Polishing is the next step after grinding. All the components were polished with the help of the auto polisher machine, where diamond liquid solution used.
7. All the components were optically inspected in the optical microscope and scanning electron microscope to find the failure mode and mechanism.

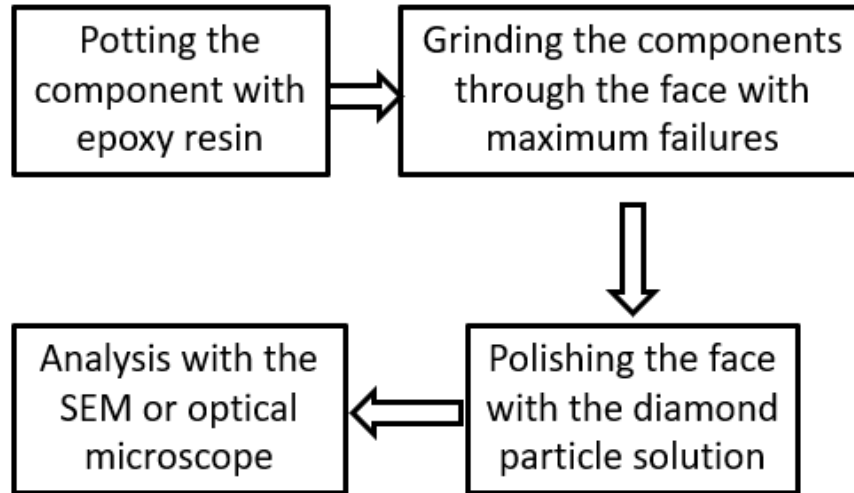


Figure 26: Steps for performing the failure analysis

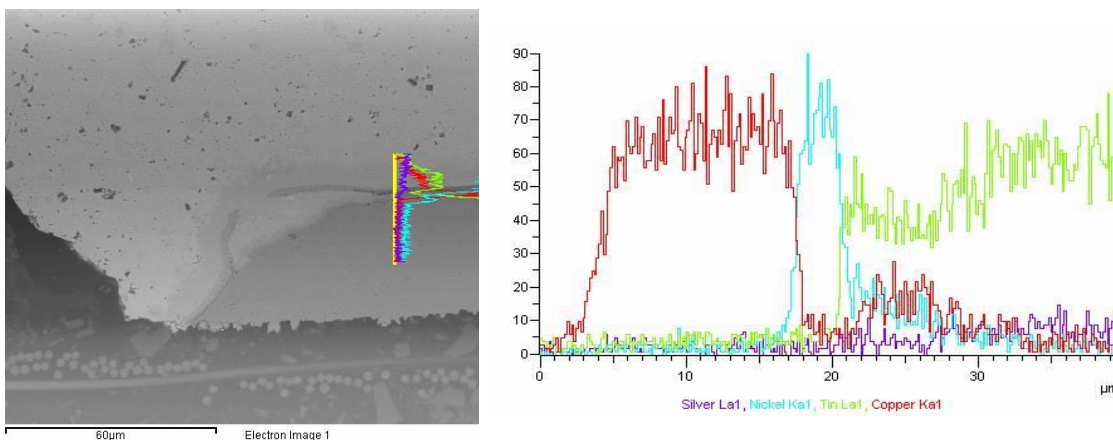
Optical Microscopy

All the failure locations that were found through the probing were analyzed for different modes and mechanisms under the SEM. There are different things that can be analyzed under the SEM or optical microscope like

1. The failure modes and mechanisms that occurred during the accelerated life cycle testing.
2. EDS analysis for the confirmation of the nickel barrier

EDS Analysis for all the Packages

Energy dispersive X-ray spectroscopy is a type of analysis to find out the material composition. All the components on the test board were tested for the presence of nickel barrier on both the package and board sides. This is done to verify the Nickel barrier on the package and board side of the component. During a thermal cycling conditions because of the continuous stresses applied on the component for a period, there will be formation of the intermetallic. The nickel barrier will prevent the formation of the intermetallic for some time. After a period, due to this continuous expansion and contraction of the solder balls there will be a breach in the nickel barrier which causes the formation of the intermetallic.

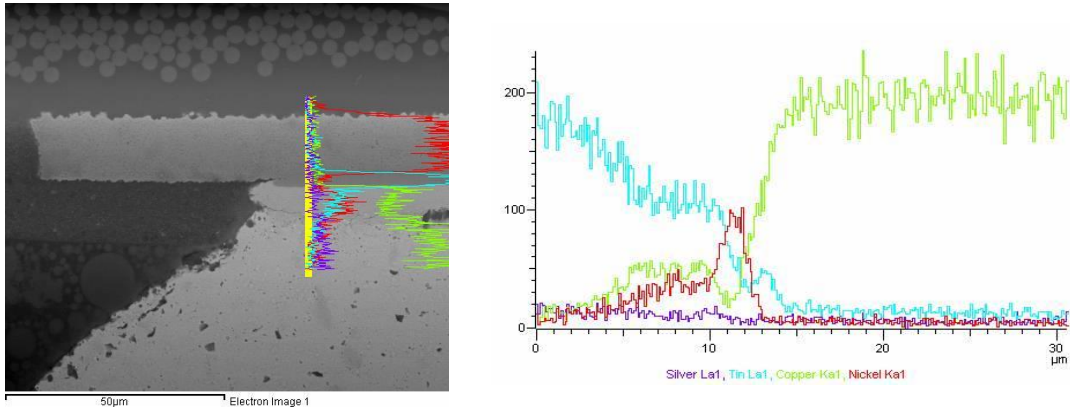


BGA 676 Board side

Figure 27: EDS analysis on the board side of the package for the verification of the nickel barrier

In the figure 27 on the board side of the package due to continuous application of the stresses in the thermal cycling there is a breach in the nickel barrier. This breach created a path for the formation of the intermetallic, which is the combination of the copper

and tin. This analysis was performed to see the consistency in different packages i.e. whether all the packages consists the nickel barrier or not.



BGA 676 Component Side

Figure 28: EDS analysis on the component side of the package for the verification of the nickel barrier

Figure 28 explains the breach in the nickel barrier on the package side also. Creating the path for the formation of the IMC. This phenomenon is further explained through the cross-sectional analysis.

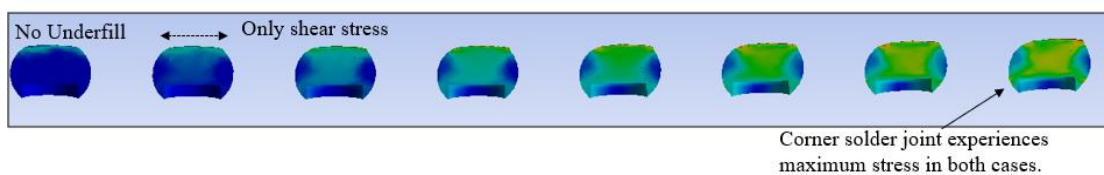
EDS analysis verified that all the packages that were considered for the experiment consists of the nickel barrier and the early failures in the packages are not due to the absence of the nickel barrier in that package.

SEM Analysis

In an experiment there are three different types of underfills selected. Each underfill has different properties range and each underfill will act differently under the thermal cycling conditions. All the four different conditions were cross sectioned separately and all the data about the failure modes and mechanisms were captured separately to make a comparison. All the failure analysis data is captured with the help of SEM, where all the failure locations were captured accurately.

No-UF condition

When there is No-UF under a BGA package the highest amount of stress will be acted on the corner most solder balls because of the combination of the global warpage and the shear stresses. Due to the absence of the underfill to support the solder balls from the warpage stresses, the corner most solder balls experienced more warpage stresses than shear. All the solder ball on the outer daisy chains experiencing maximum amount of stresses failed. In some cases, the inner solder balls also failed because of the warpage and the normal stresses that are acting on the solder balls after the first failure. Figure 29 explains the plastic work on the solder ball and the stresses acting on the corner most solder ball of the package.



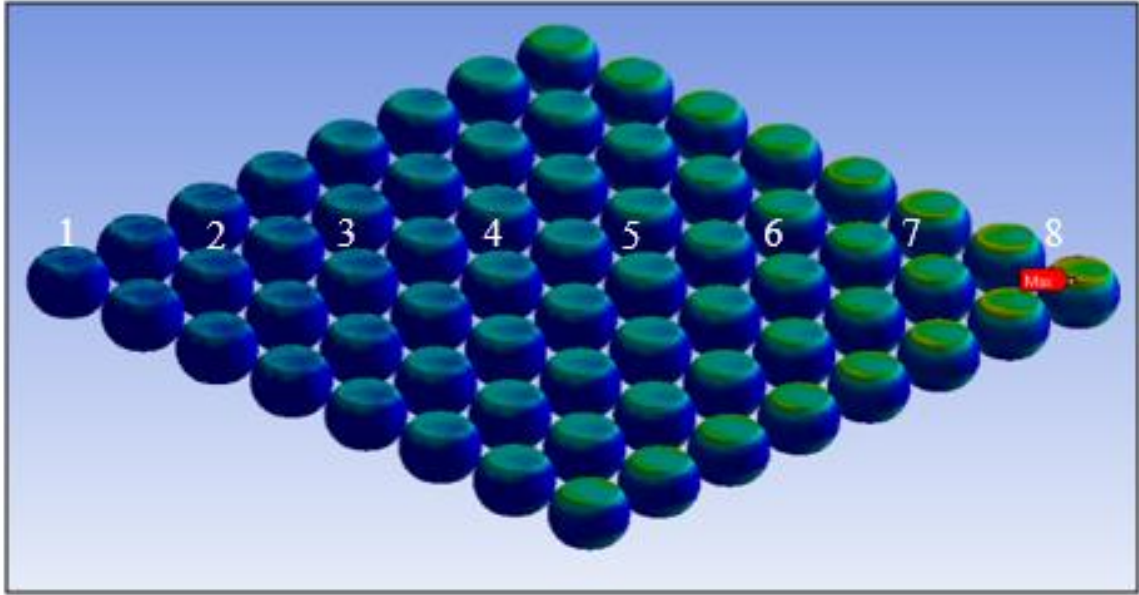
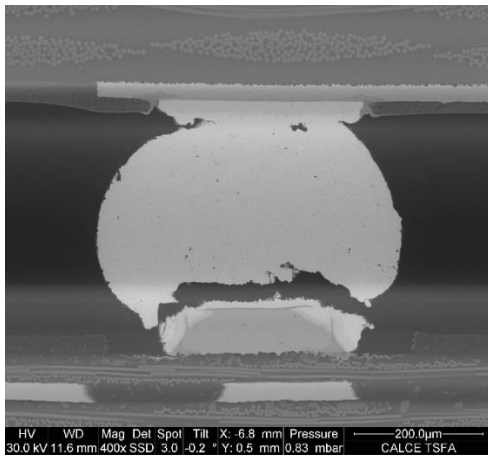
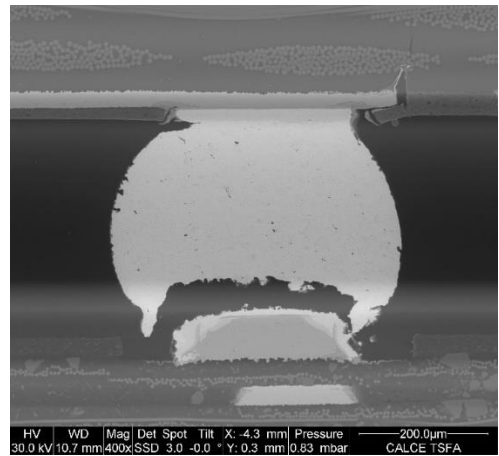


Figure 29: Plastic work across the solder ball for the No UF component to find out the critical solder ball



E01 U3 8th solder ball



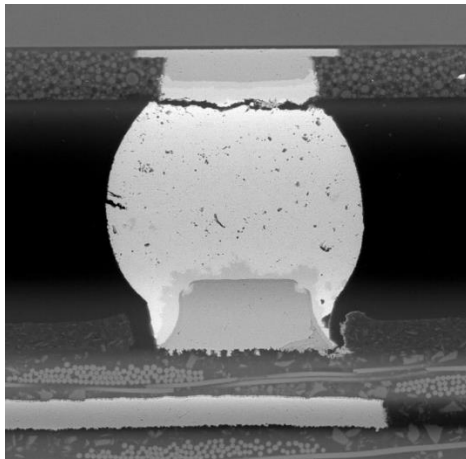
E01 U8 8th solder ball

Figure 30: Failures in the solder ball due to the warpage stresses acting on the packages

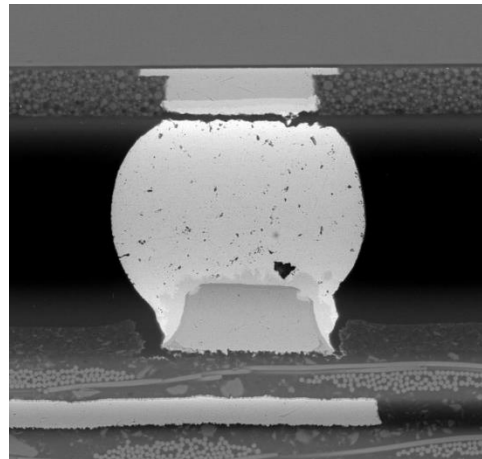
As shown in the figure 30 the maximum amount of stress is acting on the corner most solder balls of the package. Because of the warpage stresses that are acting, solder balls peeled from the bottom side of the package. The signature of the cracks suggest that

the dominant stress condition is warpage in the No-UF case. This proves that for the corner most solder balls of the package warpage played a vital role and for the high temperature applications it is important to mitigate the warpage stresses using the underfill under the BGA package. All the initial simulations were performed on the BGA 256 package. For comparison purposes all the images that are shown are of the BGA 256 package.

The TTF of the No-UF board is low. The signature of the crack is varying from package to package and from the DNP. It also depends on the location of the package on the board and size of the package. The smaller the package size lower the effect of warpage and vice versa.



E01 U5 9th solder ball



E01 U5 11th solder ball

Figure 31: Failures in the CSP devices, the crack is initiated on the component side

The solder balls shown in the figure 31 are from the CSP devices, which is the smallest package in the experiment conducted. In the CSP devices failures are propagated on the package side of the component. This is due to the tensile stresses that are acting on

the solder balls. This hypothesis must be further verified from the FEA simulations. This research is mostly concentrated on the properties of the material. This might be the next step to move forward with this research work.

Lord Material

Lord is corner bonded material which has low T_g , high modulus and low CTE. Because of its higher modulus, it can only be used as a corner bonded material. It is filled using an ordinary capillary filling. Two boards were taken in the experiment with the corner bonded material, both the boards failed early compared to the rest of the boards in the experiment. These boards were taken out early to find out the exact failure modes and mechanisms at the time of failure.

Although corner bonded material which has higher modulus mitigates the warpage issues on the components, it exerted more amount of stresses on the corner solder balls which results in the failure of the components in the early stages of the experiment.

Figure 32 shows the failure locations in BGA 192 package found through probing.

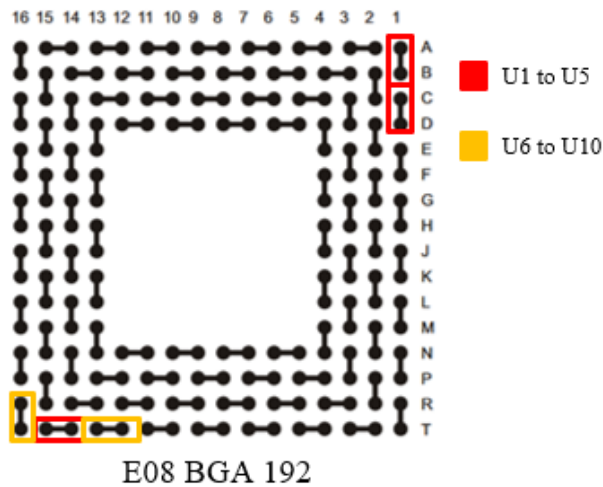
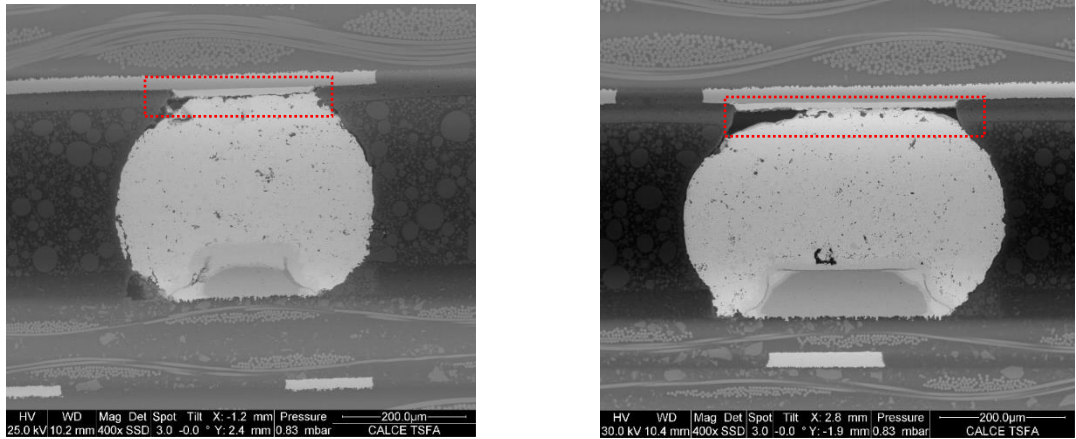


Figure 32: Failures in the lord material packages, as they are concentrated on the corners of the package

Cracks are propagated from the package side of the component and all the cracks are near the interface between the solder ball and the copper pad suggesting the tensile stresses that are acting on the solder ball. Figure 33 shows some of the solder balls with crack initiations on the package side of the component.



E08 U3 BGA192

E08 U8 BGA192

Figure 33: Failures occurred in the solder balls due to the tensile stresses in the lord material packages

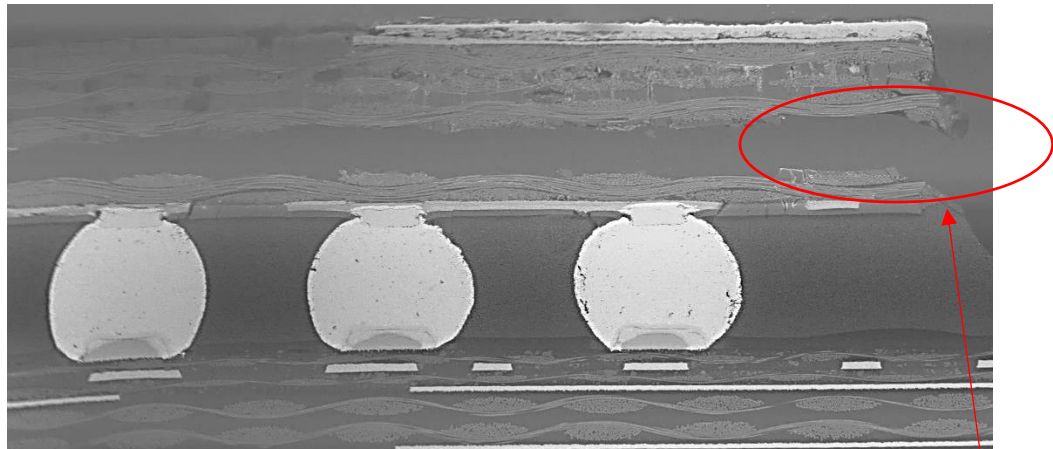
Henkel Material

Henkel is one of the fully filled underfills under the BGA packages. There are four test boards filled with this type of underfill. This material has moderate T_g , moderate modulus and low CTE. The curing time for this material is low. It will work well with the manufacturing and assembling times of the components in the assembly processes. This material gave the highest TTF for almost all the components. All the uncertainties found in the Weibull analysis will be explained in this section.

Early failures

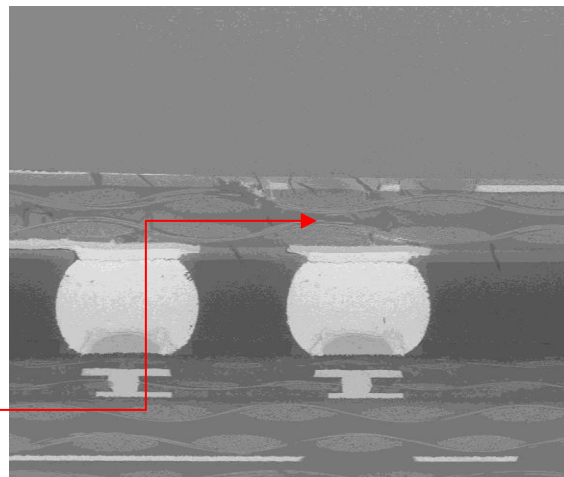
Some of the Henkel based components showed early failures in the thermal cycling conditions. All the components were identified and cross sectioned. The analysis found

that these early failures were attributed to the longitudinal cracks in the substrate, tearing the components apart at the top. This may be due to the degradation of the substrate over the period or the faulty components at the time of the assembly. This type of signature is only observed in these components.



E09 & E12 BGA 676

Substrate tear down



Delamination of the substrate

E12 BGA 192

Figure 34: Early failure in the Henkel material due to weak substrate

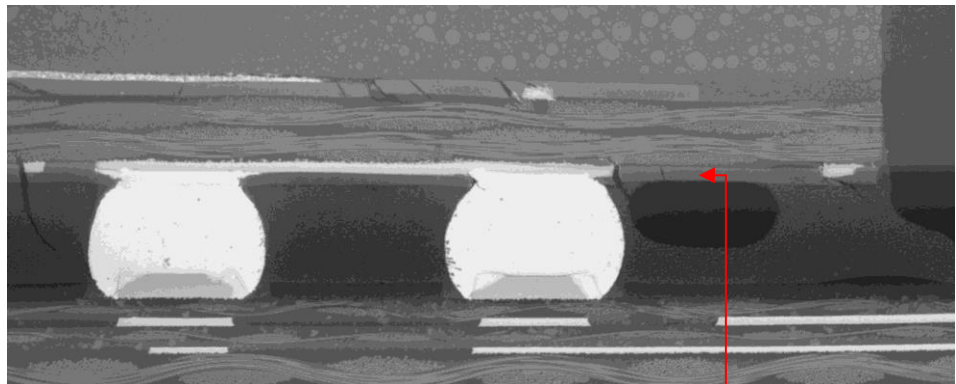
The degradation of the substrate was due to the weak substrate. Figures 34 shows a tear down and the delamination of the substrate. These tear down and delamination might had disrupted the copper traces in the substrate resulting in the early failures of the

components. There are no solder ball failures in these components, resulting to these conclusions that was mentioned above.

Voiding

In the Henkel material there is very low void percentage compared to all the underfills. But there are some voids which resulted in the cracks that propagated through the substrate and the solder balls.

Voiding is an important issue in any of the thermal cycling condition. As it will disrupt the basic purpose of the underfill. The underfills are used to create a uniform isotropic material which will reduce the stresses acting on the solder balls. The stress concentrations near the voids are varying, resulting in delamination and cracks. The changes in the stress concentrations near the edges of the voids will act as a source for the crack initiation. The initiated crack will pass through the solder ball resulting in the failure of the solder ball.



E09 U2

Cracks that are initiated from voids

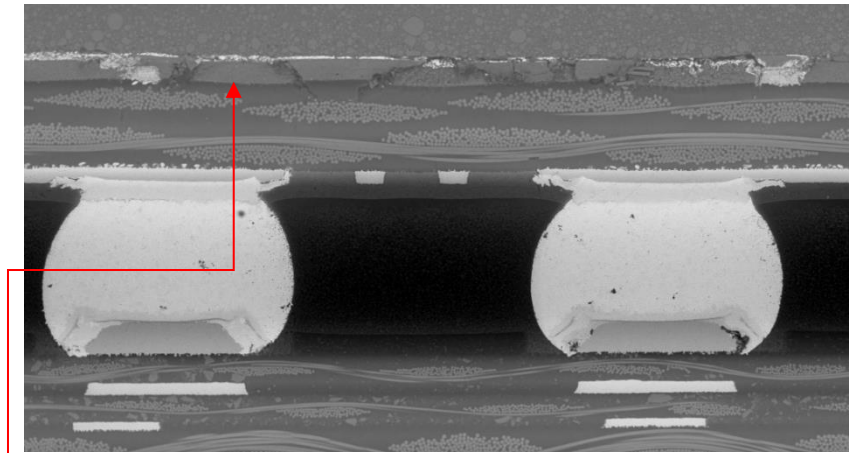
Figure 35: Voids present under the package with the Henkel underfill

The figure 35 shows the crack that is initiated from the void and passes through the substrate. The number of voids in the Henkel material was far less than the other

materials that were tested. Although there is some void percentage that is there in the underfill there are very few solder ball failures found in the packages with Henkel material.

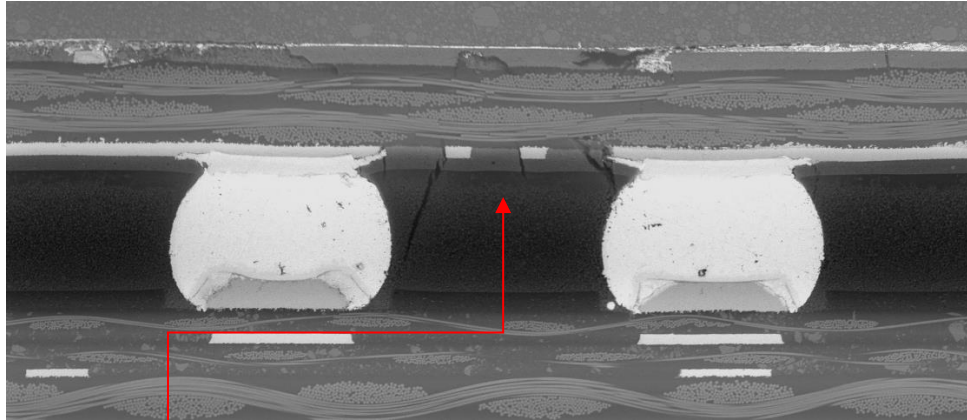
Die attach and Underfill cracks

In most of the cases the failures are not in the solder balls but near the other areas of the package like the die attach or the substrate. The underfill has done its intended function of reducing the stresses that were acting on the solder balls. Over a period, the stresses that were acting on the package accumulates, resulting in the cracks near the die attach and the substrate. Figure 36 will explain the failures in the die attach and the substrate.



Die Attach
Cracks

E09 U2



Underfill Cracks

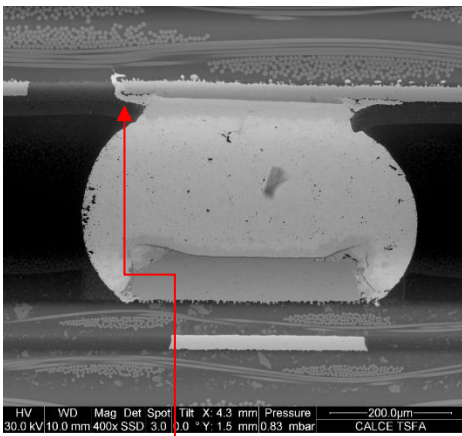
E09 U2

Figure 36: Cracks found in the die attach and the underfill in the failure analysis

The cracks were also initiated in the underfill and they were propagated towards that substrate. These cracks are due to the continuous expansion and contraction of the underfill over a period and the global warpage of the board, resulting in application of stresses on the underfill and initiating the crack.

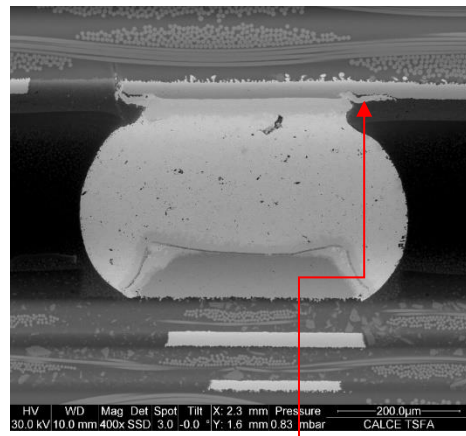
Solder Extrusion

This is a different type of phenomenon that was seen only in the Henkel material components. The solder is extruded into the underfill and the substrate. As the components goes through thermal cycling the solder material will change its state from solid to liquid, and the underfill material will continuously contract and expand. After a period when there is small crack formation and the temperature is high. The underfill material expands and pushes the liquidus solder material into the cracks resulting in the extrusions that are seen in the figure 37.



Extrusion of the solder material into the cracks

E03 U2



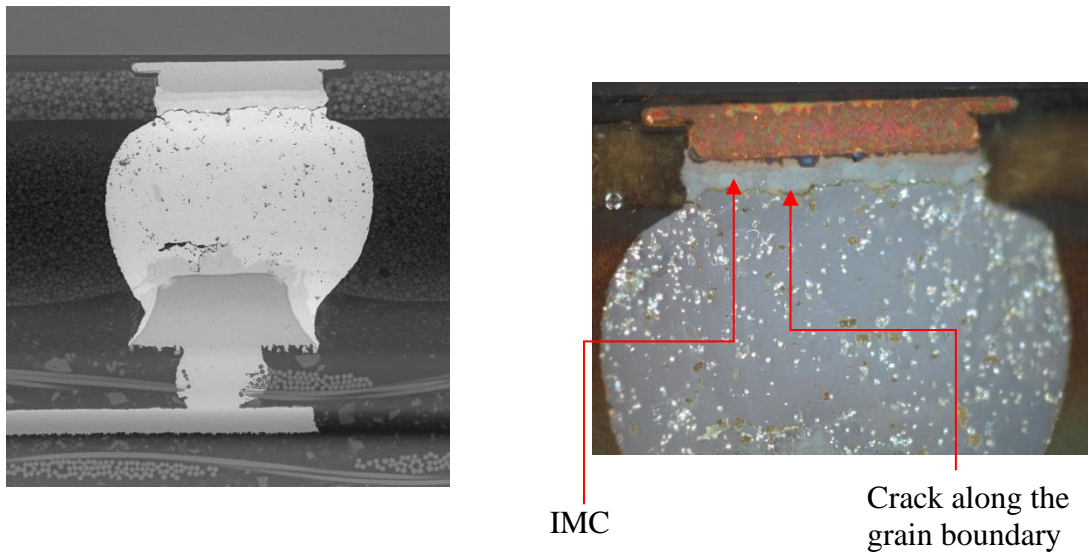
Extrusion of the solder material into the cracks

Figure 37: Solder extrusions found on the component side due to the continuous expansion and contraction of the underfill

Solder ball failures

In most of the cases there are no failures in the solder balls in the packages with the Henkel materials, but there are some cracks that are initiated near the interface between the solder ball and the copper pad. This is due to the combination of the shear and tensile stresses that are acting on the solder balls during the thermal cycling.

In the figure 38 the crack is propagated from the package side. The zigzag pattern of the crack suggests that the crack is propagating through the grain boundaries. To verify this theory the package is analyzed under the polarized light to identify the grain boundaries in the solder balls. This is shown in the figure 38.



CSP 144 E03 U6

Figure 38: Solder ball failures found in the Henkel material packages due to the combination of shear and tensile stresses

Sanyu Material

Sanyu is the second fully filled underfill material. It has high T_g , high modulus and low CTE than the Henkel material. It is a type of material which showed a good TTF at the start of the experiment but varied at the time of completion. There are different failure modes that were found during the analysis.

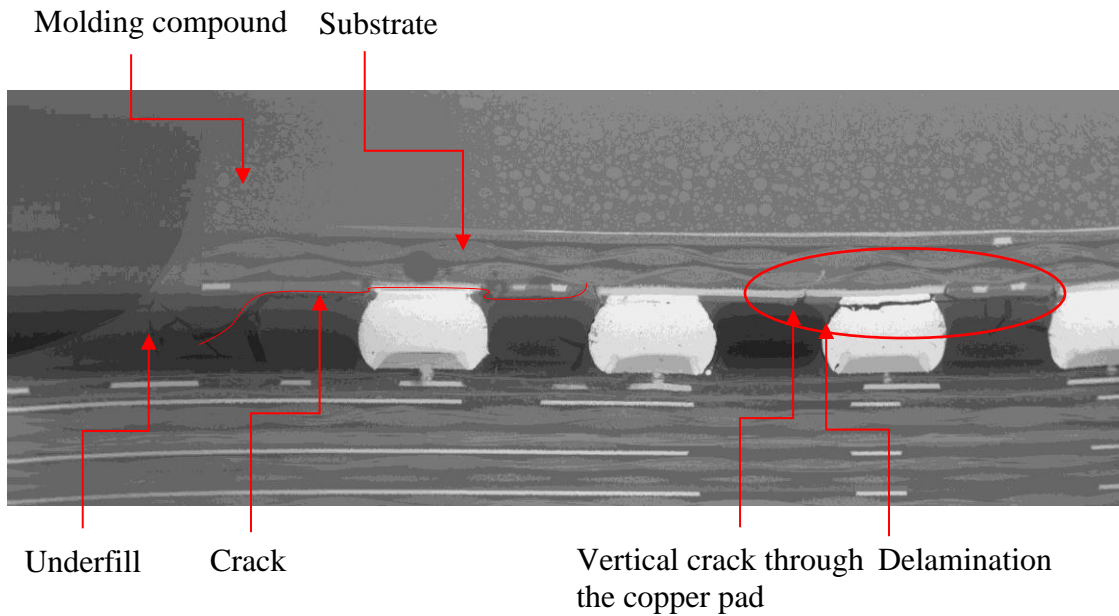


Figure 39: Failure sites found in the packages with Sanyu material under the thermal cycling

Underfill degradation

The Sanyu material degraded as the underfill undergoes thermal cycling. Due to the degradation there might be reduction in the fracture toughness of the material, due to which cracks were initiated in the underfill and propagated through the solder ball forming a continuous crack as shown in the figure 39. This degradation may be due to the change in the material properties over a period, an additional aging test was performed to verify the hypothesis will be explained in the next section. Due to global warpage stresses acting on the underfill, the cracks were initiated in the material.

Delamination

The adhesive strength of the underfill degrades over a period when it is subjected to thermal cycling conditions. This happens because of the continuous expansion and contraction of the underfill, combined with the change in state of the solder material at higher temperatures. Resulting in delamination between the underfill and the solder ball. This delamination causes the change in the stress concentration resulting in the initiation and propagation of the crack through the solder ball. This phenomenon is observed in the Sanyu material and shown in the Figure 39.

Voiding

Sanyu material consists of highest void percentage compared to any underfill that was tested. These voids were not found during the assembly curing process. As the components undergo thermal cycling the curing of the material takes place, which makes the particles to diffuse from one place to another leaving higher void percentage in the underfill. With higher void percentage the stress concentrations that are acting on the components are completely changed resulting in the vertical cracks shown in the figure 39. Due to change in the stress concentration near the void there will be higher chances of the delamination which is shown in the figure 39.

Failure Analysis Conclusions

Both Sanyu and Henkel performed well in the thermal cycling experiment. In terms of the material Henkel with all the moderate properties performed better than the Sanyu material with high material properties by giving better support to the solder balls. Sanyu material degraded over a period resulting in crack initiation in the underfill and it has highest concentration of voids among the both, which makes it prone to unpredictable

stresses. Sanyu performed well at the start of the experiment and degraded over a period. This can be attributed to the degradation of the material properties over a period of aging. To verify this hypothesis an additional aging test was performed on both the materials to see the variance in the properties of the materials over aging.

Material Characterization

After the completion of the failure analysis to verify the hypothesis mentioned in the conclusion a material characterization study was performed. This study was done to find the effect of aging on the properties of the material.

Aging Test

An aging test was performed on both the underfill materials to check the variation in properties of the material with aging. To verify all the important properties of the material two types of test were performed, DMA and TMA. For both the test conditions 9 samples of each material was prepared. All the samples were aged at 200°C in the environmental chamber. Each sample was taken out for every 100 hours and the test was conducted till 800 hours of aging. Design of experiment data was provided in table 17.

All the samples were cured at their respective cure times that are mentioned in the data sheets. The environmental chamber was preheated to the curing temperature and the curing was performed. To reduce the variability or the chance of errors all the samples were cured at the same time.

	Henkel		Sanyu	
	DMA	TMA	DMA	TMA
Total no of samples prepared	9	9	18	18

	Henkel	Sanyu
--	--------	-------

Total no of hours of aging	800hrs	800hrs
----------------------------	--------	--------

Table 17: Design of Experiment for the aging test

TMA Testing

TMA was used to characterize the T_g , CTE1 & CTE2 of the material. This is a type of test which works on the dimensional change of the sample. The sample was subjected to a temperature ramp from room temperature to 200°C. The change in the material dimensions when a certain amount of force applied is calculated and will be plotted against the temperature to characterize the properties of the material. For this test a cubical sample of 1*1*1cm was prepared. The samples were cured in a Teflon sheet. Figure 40 shows the sample in the TMA machine.

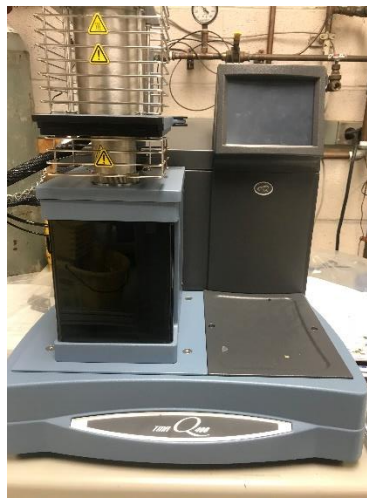


Figure 40: TMA equipment used for measuring the properties

Henkel Material

Before the testing, the time 0 samples were taken and tested for the reference purposes. They are compared to the original data sheet values. Figure 41 shows the time 0 value of the Henkel material.

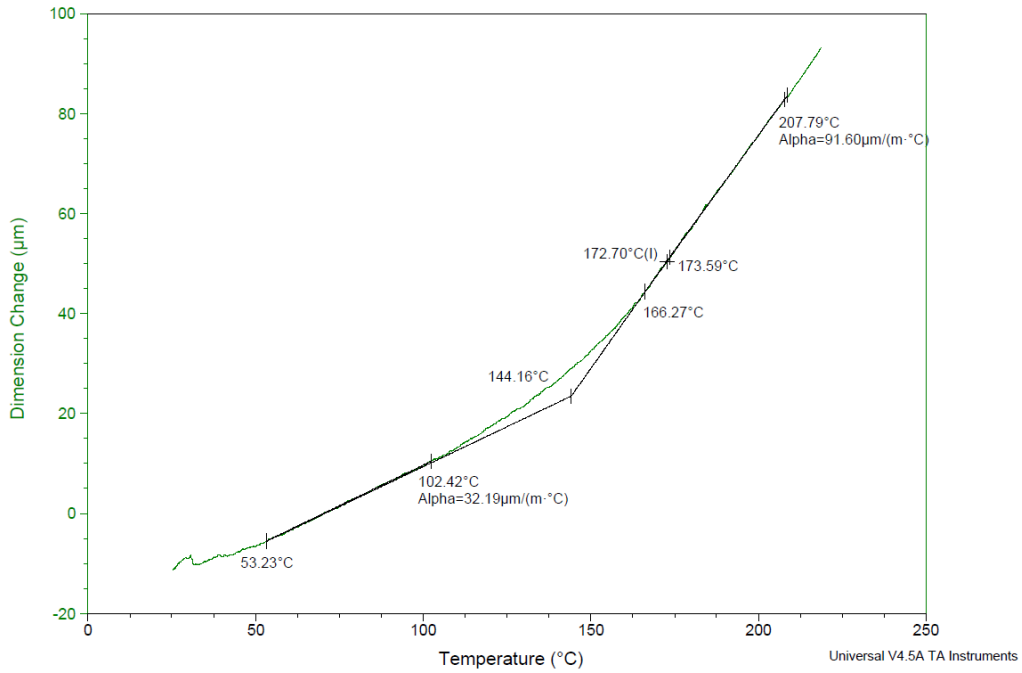


Figure 41: Time 0 TMA result of Henkel material

	CTE1	CTE2	T _g
Henkel (Data sheet)	25	58	155
Henkel (Experimental)	32.19	91.60	144.16

Table 18: Comparison between experimental and data sheet value of Henkel material

Time 0 sample of Henkel shows a slight change in the properties of the material than that of the data sheet. Experimental results show lower T_g and higher CTE1 and CTE 2 than that of the data sheet shown in table 18.

After the completion of the time 0 characterization, all the samples that were taken out from the aging test were characterized to identify the variation in the properties with aging. All the TMA results were shown in the table 19.

Henkel TMA Results			
Time	T _g	CTE1	CTE2
0 hrs	144.16	32.19	91.6
100 hrs	153.04	36.97	82.15
200 hrs	146.82	32.73	88.77
300 hrs	143.41	34.69	86.71
400 hrs	146.07	40.05	91.37
500 hrs	143.17	35.65	88.4
600 hrs	142.76	30.96	81.67
700 hrs	148.86	39.49	90.07
800 hrs	148.96	39.01	83.45
Subramani's TMA Results			
0 hrs	145	28.73	76.81

Table 19: TMA results of bulk Henkel samples aged at 200 °C

There is not much change in the T_g, CTE1 & CTE 2 in the Henkel material with aging. There is a slight reduction in CTE 2 and slight increase in the CTE 1 with aging. There is no significant change in the properties of the material with aging. A graphical representation of all the results is explained in figure 42.

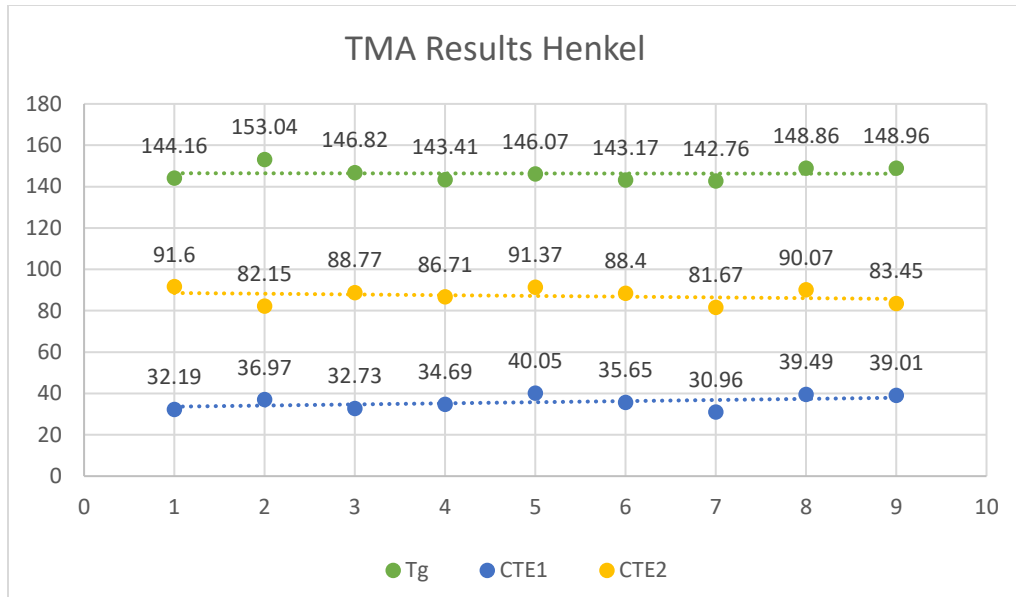


Figure 42: Graphical representation of the Henkel’s TMA results

The effect of the aging at room temperature might also affect the properties of the material. To strike out that possibility a second run of the TMA testing for the samples were done. After the samples were aged at room temperature for some time. They were tested for the same properties in TMA. The results of the second run are mentioned in the table 20.

Henkel TMA Results (2 nd run)			
Time	T _g	CTE1	CTE2
0	140.62	36.11	80.27
100	138.05	37.36	93.4
200	142.56	38.34	87.2

Table 20: TMA results of Henkel samples aged at room temperature

There is not much change in the properties of the material with aging at room temperature.

Sanyu Material

The same tests were performed on the Sanyu material also to see the variation in the properties of the material with aging. The time 0 TMA result was shown in figure 43.

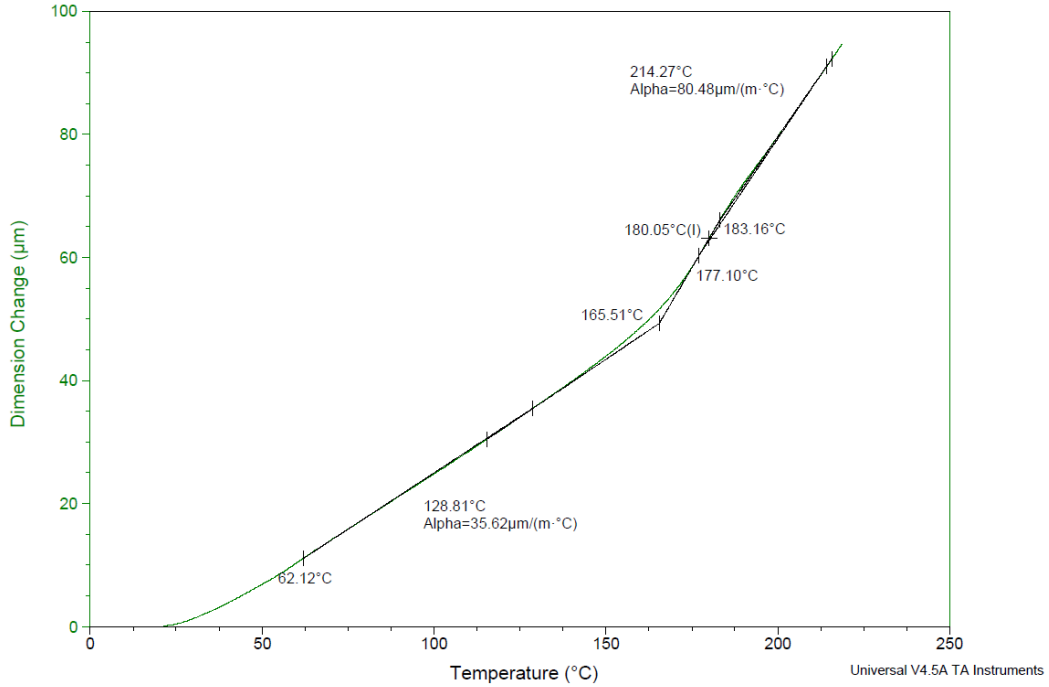


Figure 43: Time 0 TMA result of Sanyu material

	CTE1	CTE2	T _g
Sanyu (Data sheet)	25	56	196
Sanyu (Experimental)	35.62	80.48	165.51

Table 21: Comparison between experimental and data sheet value of Sanyu material

The T_g from the TMA is lower than the data sheet value and the CTE1, CTE2 are higher than the data sheet value, shown in table 21.

Sanyu material has highest T_g in all the underfills that were tested. The changes in the properties with aging might be the reason for the sudden change in failure mechanism after a few thermal cycles. This was found from the TMA testing. After the time 0 sample testing, all the other samples were tested for the properties. The results are mentioned in the table 22.

Sanyu TMA Results			
Time	T_g	CTE1	CTE2
0 hrs.	165	35.62	80.48
100 hrs.	155.17	32.6	79.12
200 hrs.	151.09	28.21	85.3
300 hrs.	151.49	34.83	84.87
400 hrs.	139.02	36.35	81.92
500 hrs.	139.61	25.97	76.26
600 hrs.	140.5	28.17	74.37
700 hrs.	132.32	27.64	73.1
800 hrs.	137.35	29.95	88.61
Subramani's TMA Results			
0 hrs.	168	31.85	97.58

Table 22: TMA results of bulk Sanyu samples aged at 200 °C

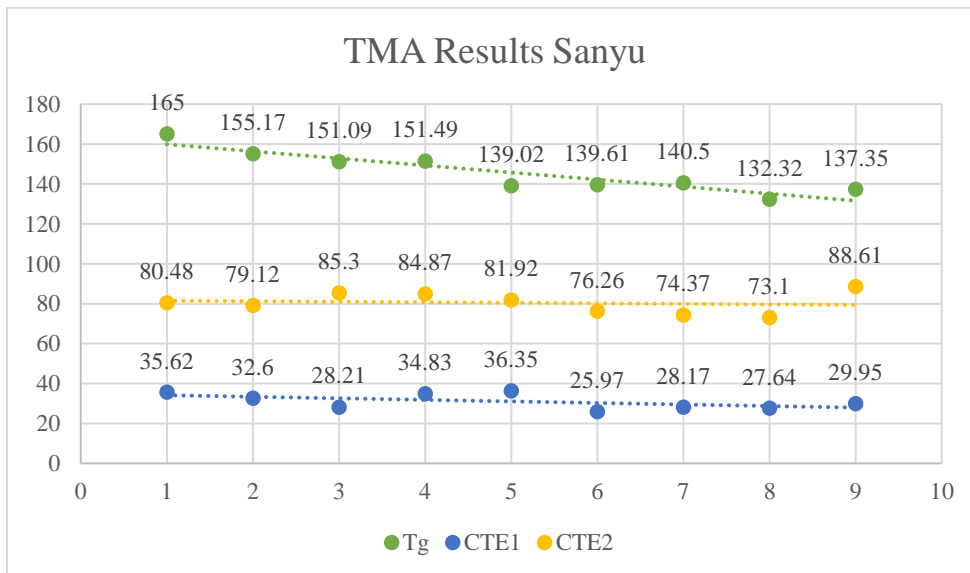


Figure 44: Graphical representation of the Sanyu TMA results

The T_g of the Sanyu material reduced over a period of thermal aging. This might be the reason for the shift in the failure mechanism. Due to the reduction in T_g there will be increase in the time at which the material is above T_g , increasing the amount of stresses acting on the solder balls. Resulting in the failures. Apart from T_g , CTE1 and CTE2 are almost the same. Figure 44 explains the graphical representation of the aging results.

DMA Testing

DMA is dynamic mechanical analyzer. It is used to characterize the properties like storage modulus and loss modulus and their dependence with temperature. The testing is mostly concentrated on the storage modulus of the material and its dependence with temperature. All the samples that were cured are grinded and molded into a thin cuboid of 30*9*0.2mm. A tensile tester was used in the DMA, the frequency sweep was done over a constant temperature to find the storage modulus of the material and it was compared to the data sheet values. Figure 45 shows the test specimen and the procedure.



Figure 45: DMA tensile testing

Henkel material

Henkel material has moderate storage modulus. A time 0 sample was taken and tested for the storage modulus. A frequency sweep from 1 to 30 Hz was performed to see the response of the storage modulus. The values were taken when the curve reaches the stagnant value. Figure 46 shows the results of the time 0 sample.

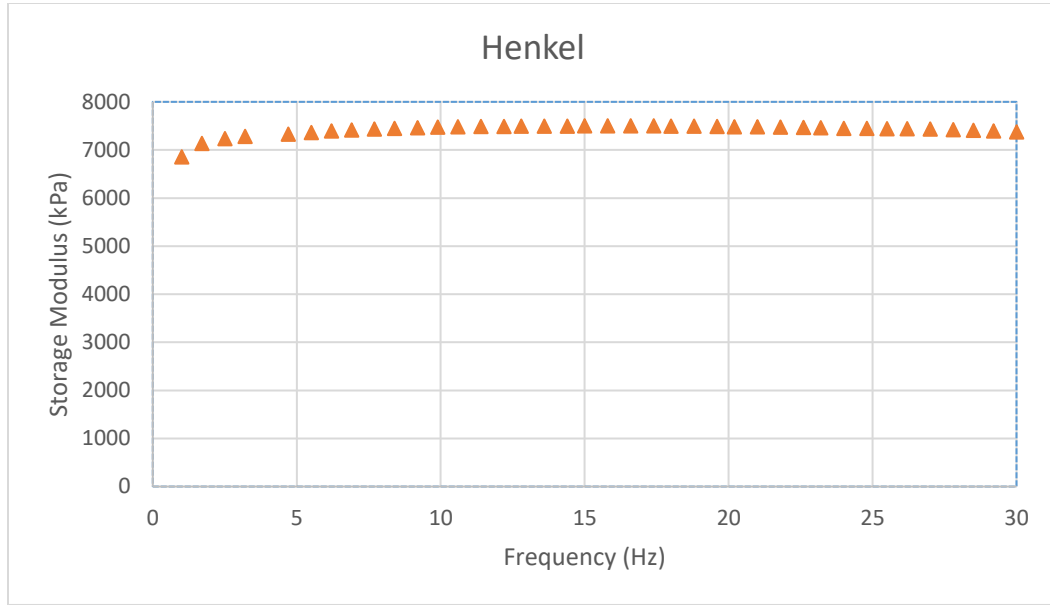


Figure 46: Time 0 DMA result of Henkel material

Storage Modulus	Data Sheet	DMA
Henkel	4.632 GPa	7.498 GPa

Table 23: Comparison between experimental and data sheet value of Henkel material

The time 0 value from the DMA shows higher storage modulus than that of the data sheet. After the Time 0 sample characterization all the other samples were grinded and characterized to find the effect of thermal aging on the storage modulus. All the results of the experiment are presented in the table 24.

DMA (Henkel)	
Time (Hours)	Storage Modulus (GPa)
Time 0	7.498
100	9.403
200	9.044
300	11.59
400	7.91
500	9.173
600	8.412
700	6.712
800	8.5

Table 24: DMA results of bulk Henkel samples aged at 200 °C

The values of the DMA testing for the storage modulus are scattered but they are all in the range of the 6.7 and the 11 GPa. The average values for the storage modulus are the same. There is not much increase in the storage modulus of the Henkel material with aging. These variations in the modulus can be attributed to the manual thin sample preparation and the error in the DMA.

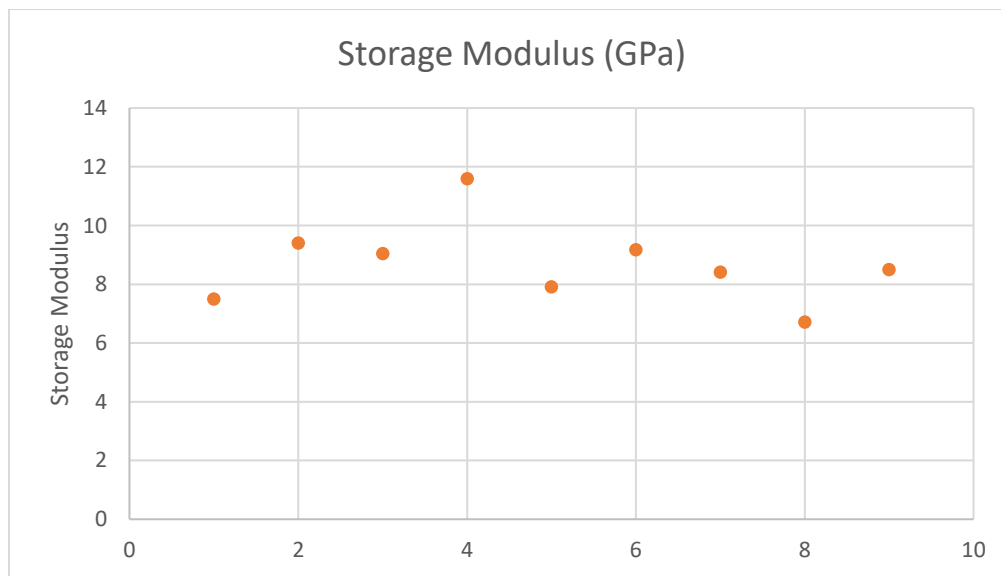


Figure 47: Graphical representation of the Henkel's DMA results

Sanyu Material

Sanyu material has the highest storage modulus among the fully filled underfills. Time 0 sample was taken, and DMA testing was performed, and the results are presented in the table 25.

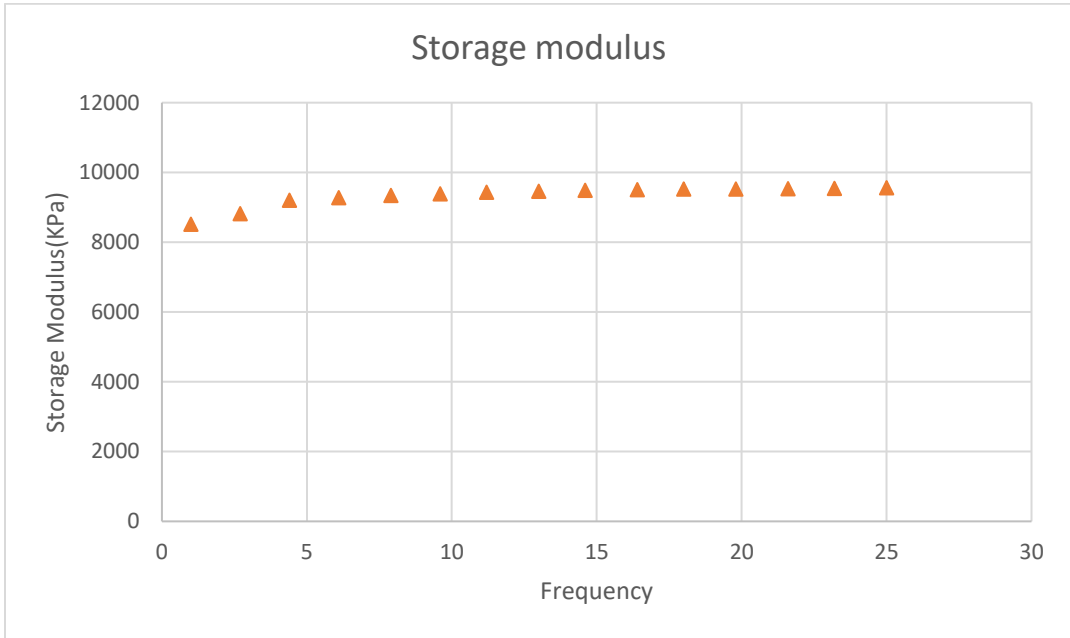


Figure 48: Time 0 DMA result of Sanyu material

Storage Modulus	Data Sheet	DMA
Sanyu	9.4 GPa	9.542 GPa

Table 25: Comparison between experimental and data sheet value of Sanyu material

The Time 0 value from the DMA is matching with the data sheet value. All the results from the DMA testing of the aged samples are presented in the table 26.

All the DMA values are varying from 9.1 to 11.2 GPa. This variation can be attributed to the manual sample preparation and minute errors in the DMA results.

DMA (Sanyu)

Time (Hours)	Storage Modulus (GPa)
Time 0	9.542
100	10.14
200	10.065
300	9.114
400	11.246
500	9.173
600	9.324
700	12.035
800	11.045

Table 26: DMA results of bulk Sanyu samples aged at 200 °C

There is a slight increase in the storage modulus with aging. But the increase in storage modulus is not significant to change the failure mechanism after a period of aging.

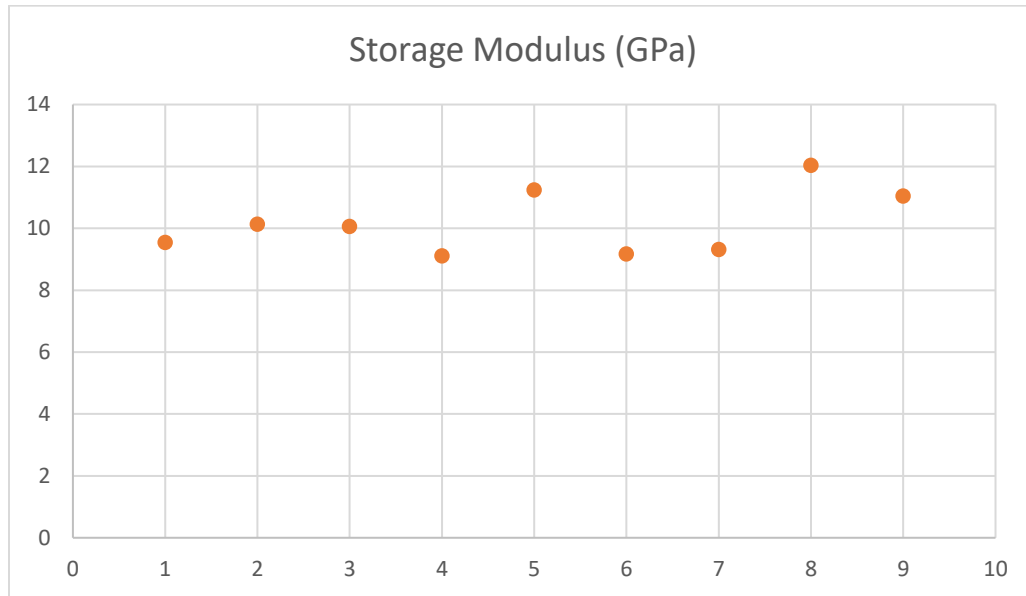


Figure 49: Graphical representation of the Sanyu DMA results

Hypothesis

After the experimentation there is a significant change in T_g with aging. This explains the change in the failure mechanism of the Sanyu after a few thermal cycles.

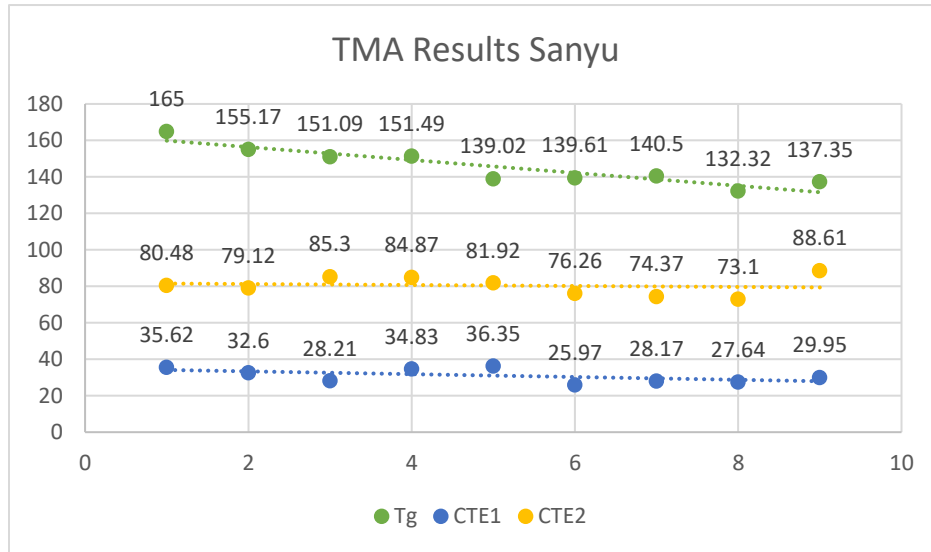


Figure 50: Graphical representation of the TMA results showing the reduction in T_g over a period of aging in Sanyu material

The T_g of the Sanyu material reduced from 165°C to 137.35°C after aging. The reduction in T_g will increase the amount of stresses acting on the package. As the T_g decreases the time that the package spend above the T_g in a thermal cycle will increase, resulting in increase in the stresses due to CTE2. There will be a point at which this shift might be occurring, this point is the time at which the change in the failure mechanism had occurred in the experiment.

To verify this hypothesis FEA simulation was performed, which will be explained in the next section.

Verification

A FEA analysis was performed with the varied properties found through the aging experiment. It was found from the FEA that with the reduction in T_g there is reduction in the TTF of the package under the same thermal cycling condition. It proves that with the reduction in the T_g there is an increase in the amount of stresses resulting in the failure of the solder balls. The results of the FEA is presented in figure 51.

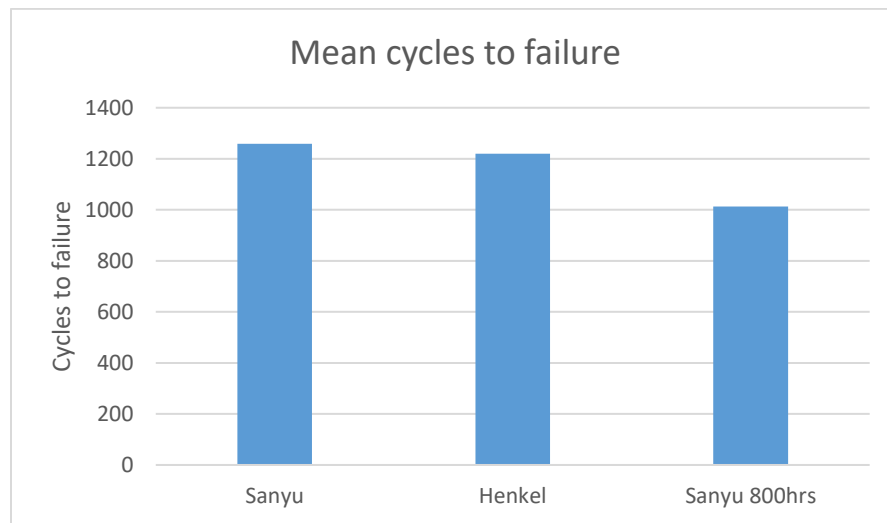


Figure 51: TTF values of the BGA packages with the changed material properties

Conclusions

Guidelines for selecting the underfills

- Underfills with relatively low CTE, High Modulus and High T_g performs better in high temp application.
 - T_g of the material should be carefully taken into consideration, as it will increase the stresses that are applying on the solder balls over a thermal cycle.

- High Tg materials will work better at low thermal cycling conditions also as the range above Tg will not be reached, which will reduce the stresses that are acting on the solder balls.
- The high modulus of the materials will exert higher amount of stresses on the die, so the combination of the material properties should be taken into consideration. In the research, materials in the range from 6 to 9.4 GPa was tested. Above that modulus there will be additional stresses acting on the die, which cause the die crack problems.
- Although these properties were for the idealized case, the variation in the properties due to aging should be taken into consideration, when the underfills were undergoing high thermal cycling conditions.
- Degradation of the underfill should be taken into consideration over a period, as the toughness will be reduced if the underfill degraded.

Contributions

- First study to characterize high Tg underfill reliability relative to low Tg underfill reliability
- First study to identify the critical characteristics (modulus, CTE) related to high Tg underfill reliability
- First study to recognize the effect of thermal aging on changes in the properties, reliability, and failure mechanism of high Tg underfills.

- Created comprehensive guidelines for selecting underfill for high temperature applications.

Bibliography

- [1] Steinberg DS. Vibration analysis for electronic equipment. United States of America: John Wiley & Sons; 2000 Jun. P. xviii.
- [2] Vandavelde, B., M. Lofrano, and G. Willems. "Green mould compounds: Impact on second level interconnect reliability." In *Electronics Packaging Technology Conference (EPTC), 2011 IEEE 13th*, pp. 283-288. IEEE, 2011.
- [3] Parker, Richard, Richard Coyle, Gregory Henshall, Joe Smetana, and Elizabeth Benedetto. "iNEMI Pb-Free Alloy Characterization Project Report: Part II–

Thermal Fatigue Results for Two Common Temperature Cycles." *Proceedings of SMTAI 2012* (2012): 348-358.

- [4] P. Rajmane et al., "Failure mechanisms of boards in a thin wafer level chip scale package," 2017 16th IEEE Intersociety Conference on Thermal and Thermomechanical Phenomena in Electronic Systems (ITherm), Orlando, FL, 2017, pp. 1099-1105, doi: 10.1109/ITHERM.2017.7992611.
- [5] Abhishek Nitin Deshpande, "Comprehensive design analysis of thick FR-4 QFN assemblies for enhanced board level reliability", The University of Texas at Arlington August, vol. V, pp. 5, 2015.
- [6] Sharon, G. Thermal Cycling and Fatigue. DfR Solutions. White Paper. 2015
- [7] Performance Test Methods and Qualification Requirements for Surface Mount Solder Attachments, IPC Standard 9701A, 2002.
- [8] Serebreni, Maxim, and Greg Caswell. "The Impact of Glass Style and Orientation on the Reliability of SMT Components." In *International Symposium on Microelectronics*, vol. no. 1, pp. 699-706. International Microelectronics Assembly and Packaging Society, 2018.
- [9] Davis, E. M., William E. Harding, Robert S. Schwartz, and John J. Corning. "Solid logic technology: versatile, high-performance microelectronics." *IBM Journal of Research and Development* 8, no. 2 (1964): 102-114.
- [10] Okura, J. H., S. Shetty, B. Ramakrishnan, A. Dasgupta, J. F. J. M. Caers, and T. Reinikainen. "Guidelines to select underfills for flip chip on board assemblies and compliant interposers for chip scale package assemblies." *Microelectronics Reliability* 40, no. 7 (2000): 1173-1180.
- [11] Shi HB, Ueda T. Mitigation of thermal fatigue failure in fully underfilled lead-free array-based package assemblies using partial underfills. Electronics Packaging Technology Conference (EPTC), 2011 IEEE 13th 2011 Dec 7 (pp. 542-547). IEEE.
- [12] Lee JY, Hwang TK, Kim JY, Yoo M, Sohn ES, Chung JY, Dreiza M. Study on the board level reliability test of package on package (PoP) with 2nd level underfill. In Electronic Components and Technology Conference, 2007. ECTC'07. Proceedings. 57th 2007 May 29 (pp. 1905-1910). IEEE.
- [13] Ho, P. S., Z. P. Xiong, and K. H. Chua. "Study on factors affecting underfill flow and underfill voids in a large-die flip chip ball grid array

- (FCBGA) package." In *Electronics Packaging Technology Conference, 2007. EPTC 2007. 9th*, pp. 640-645. IEEE, 2007.
- [14] Fan, X-J., H. B. Wang, and T. B. Lim. "Investigation of the underfill delamination and cracking in flip-chip modules under temperature cyclic loading." *IEEE Transactions on Components and Packaging Technologies* 24, no. 1 (2001): 84-91.
- [15] Zhang, Xiaowu, C. Q. Cui, K. C. Chan, E. H. Wong, and Mahadevan K. Iyer. "Analysis of solder joint reliability in flip chip package." *International Journal of Microcircuits and Electronic Packaging* 25, no. 1 (2002): 147-159.
- [16] Paquet, M-C., Michael Gaynes, Eric Duchesne, David Questad, Luc Bélanger, and M. Sylvestre. "Underfill selection strategy for Pb-free, low-K and fine pitch organic flip chip applications." In *Electronic Components and Technology Conference, 2006. Proceedings. 56th*, pp. 9-pp. IEEE, 2006.
- [17] Hannan, Nael, and Puligandla Viswanadham. "Critical aspects of reworkable underfills for portable consumer products." In *Electronic Components and Technology Conference, 2001. Proceedings., 51st*, pp. 181-187. IEEE, 2001.
- [18] Lau, John, Jeffery Lo, Jimmy Lam, Eng-Leong Soon, Woai-Sheng Chow, and Ricky Lee. "Effects of Underfills on the Thermal-Cycling Tests of SnAgCu PBGA (Plastic Ball Grid Array) Packages on ImAg PCB (Printed Circuit Board)." In *Electronics Packaging Technology Conference, 2007. EPTC 2007. 9th*, pp. 785-790. IEEE, 2007.
- [19] B. Noh, J. Yoon and S. Jung, "Effects of Underfill Materials and Thermal Cycling on Mechanical Reliability of Chip Scale Package," in *IEEE Transactions on Components and Packaging Technologies*, vol. 32, no. 3, pp. 633-638, Sept. 2009, doi: 10.1109/TCAPT.2008.2010503.
- [20] N. Islam, A. Syed, T. Hwang, Y. Ka and W. Kang, "Issues in fatigue life prediction model for underfilled flip chip bump," *2011 IEEE 61st Electronic Components and Technology Conference (ECTC)*, Lake Buena Vista, FL, 2011, pp. 767-774, doi: 10.1109/ECTC.2011.5898599.
- [21] T. Burnette, Z. Johnson, T. Koschmieder and W. Oyler, "Underfilled BGAs for ceramic BGA packages and board-level reliability," 2000 Proceedings. 50th Electronic Components and Technology Conference (Cat.

No.00CH37070), Las Vegas, NV, USA, 2000, pp. 1221-1226, doi: 10.1109/ECTC.2000.853329.

- [22] H. Shi, C. Tian, M. Pecht and T. Ueda, "Board-level shear, bend, drop and thermal cycling reliability of lead-free chip scale packages with partial underfill: a low-cost alternative to full underfill," 2012 IEEE 14th Electronics Packaging Technology Conference (EPTC), Singapore, 2012, pp. 1-12, doi: 10.1109/EPTC.2012.6522604.
- [23] Shi HB, Ueda T. Mitigation of thermal fatigue failure in fully underfilled lead-free array-based package assemblies using partial underfills. In Electronics Packaging Technology Conference (EPTC), 2011 IEEE 13th 2011 Dec 7 (pp. 542-547). IEEE.
- [24] Williams, C., Tan, K. E., & Pang, J. H. (2010, June). Thermal cycling fatigue analysis of SAC387 solder joints. In *Thermal and Thermomechanical Phenomena in Electronic Systems (ITherm)*, 2010 12th IEEE Intersociety Conference on (pp. 1-7). IEEE.
- [25] A. Deshpande, H. Khan, F. Mirza and D. Agonafer, "Global-local finite element optimization study to minimize BGA damage under thermal cycling," Fourteenth Intersociety Conference on Thermal and Thermomechanical Phenomena in Electronic Systems (ITherm), Orlando, FL, 2014, pp. 483-487.
- [26] S. Krishnamurthy, A. Deshpande, Md Malekkul Islam and D. Agonafer, "Multi design variable optimization of QFN package on thick boards for enhanced board level reliability," 2016 15th IEEE Intersociety Conference on Thermal and Thermomechanical Phenomena in Electronic Systems (ITherm), Las Vegas, NV, 2016, pp. 1546-1550.
- [27] P. Rajmane, MULTI-PHYSICS DESIGN OPTIMIZATION OF 2D AND ADVANCED HETEROGENOUS 3D INTEGRATED CIRCUITS, Arlington, Texas:University of Texas at Arlington, 2018.

